A general class of non-linear kinematic models to predict mean stress relaxation and multiaxial ratcheting in fatigue problems – Part I

Marco Antonio Meggiolaro[*,1], *Jaime Tupiassú Pinho de Castro*[1], *Hao Wu*[2]
[1]Department of Mechanical Engineering, Pontifical Catholic University of Rio de Janeiro, Brazil
[2]School of Aerospace Engineering and Applied Mechanics, Tongji University, Shanghai, PR China
meggi@puc-rio.br, jtcastro@puc-rio.br, wuhao@tongji.edu.cn

Abstract

Ratcheting is a gradual accumulation of plastic strain that can influence fatigue lives of structural components due to the premature exhaustion of the material ductility, much earlier than predicted by traditional fatigue crack initiation models. Ratcheting is usually associated with a significant mean stress component in either uniaxial or multiaxial stress-controlled histories. The very same process can induce mean stress relaxation in strain-controlled histories, affecting fatigue lives due to consequent mean or maximum stress effects. Such processes are mainly caused by a local distortion of the yield surface, which would require the use of complex yield functions other than von Mises' to be properly described. The addition of non-linear terms to the kinematic hardening rules compensates for this requirement, rendering it possible to model ratcheting effects using the von Mises yield function without dealing with distortion. In this two-part work, the formulation of the main non-linear kinematic (NLK) models is unified into a generalized equation, represented using engineering notation in a reduced-order five-dimensional (5D) space that may lower in half the associated computational cost. Part I introduces the proposed 5D stress and strain spaces, which are a scaled version of Ilyushin's 5D spaces. These 5D spaces are then applied to the qualitative study of uniaxial ratcheting, multiaxial ratcheting, and mean stress relaxation. Part II of this work derives all incremental plasticity equations from the NLK approach in the spaces proposed in Part I, and discusses its advantages over the classical 6D formulation. These NLK models are then used in Part II to quantitatively predict uniaxial ratcheting, multiaxial ratcheting, and mean stress relaxation, validated from experiments with 316L steel cylindrical and tubular specimens.

Keywords: Multiaxial fatigue; Ratcheting; Incremental plasticity; Non-linear kinematic hardening; Non-proportional loading.

1. Introduction

Ratcheting, sometimes called cyclic creep, is the gradual accumulation of any plastic strain component with increasing number of cycles [1]. Although this phenomenon is activated by cyclic plastic loading, it leads to a steady straining in a certain direction that can affect the fatigue life of structural components due to the premature exhaustion of the material ductility, much earlier than its usual crack initiation life. It can happen independently of temperature, even though temperature effects can influence ratcheting by changing the yield strength and the hardening or softening behavior of the material.

Ratcheting is usually associated with uniaxial or multiaxial load histories containing mean stress components. Any loading history that triggers the unsteady effects associated with ratcheting is called

[*] Corresponding author. Tel.: +55-21-3527-1424; fax: +55-21-3527-1165. *E-mail:* meggi@puc-rio.br

an *unbalanced* history. Balanced histories, on the other hand, can also present complex transient elastoplastic hysteresis loops due to strain hardening or softening effects, however after them the material behavior involves a closed elastoplastic loop, with no net accumulation of plastic deformation.

In unbalanced histories, plastic strain accumulation can continue even after the strain hardening or softening transient ends, generating hysteresis loops that do not fully close. But ratcheting rates may decay as a function of the accumulated plastic strain, until reaching stabilized closed hysteresis loops, in a *plastic shakedown* process. In some cases, it is possible that the steady-state is not only a closed loop but it is also perfectly elastic, in which case the transient behavior is called *elastic shakedown*.

There are two main types of ratcheting: uniaxial and multiaxial. The first is caused by an unbalanced uniaxial (or any other proportional) history, while the latter requires unbalanced multiaxial non-proportional (NP) conditions, both under stress control. If, on the other hand, the load history is under strain control, then the same microstructural mechanisms that cause uniaxial or multiaxial ratcheting are responsible for gradually reducing mean stress components towards zero. This phenomenon, called *mean stress relaxation*, can be interpreted as an inverse ratcheting problem, and may be present in both uniaxial and multiaxial strain-controlled histories.

In Part I of this two-part work, reduced-order five-dimensional (5D) stress and strain spaces are proposed, which significantly decrease the computational cost in the incremental plasticity formulations required to predict the material behavior subjected to unbalanced stress or strain histories. Its application to the qualitative description of ratcheting and mean stress relaxation is discussed, while quantitative evaluations are the subject of Part II, which derives the NLK incremental plasticity equations in the proposed 5D spaces. The 5D representation of stresses and strains is presented next.

2. Five-dimensional stress and strain formulation

2.1 Voigt-Mandel's notation

Stress and strain tensors can be represented as nine-dimensional (9D) vectors [2], avoiding the need to work with tensor operations. Even better representations were proposed by Voigt and Mandel [3], taking advantage of shear symmetries to express the stress or strains as six-dimensional (6D) vectors. Denoting σ_i and s_i as the stress components and their deviatoric parts, and analogously ε_i and e_i for the strain components, then Voigt-Mandel's vector representation of the stresses, strains, deviatoric stresses, and deviatoric strains used in this work become

$$\begin{cases} \vec{\sigma} = \left[\sigma_x \quad \sigma_y \quad \sigma_z \quad \tau_{xy}\sqrt{2} \quad \tau_{xz}\sqrt{2} \quad \tau_{yz}\sqrt{2} \right]^T \\ \vec{\varepsilon} = \left[\varepsilon_x \quad \varepsilon_y \quad \varepsilon_z \quad \gamma_{xy}/\sqrt{2} \quad \gamma_{xz}/\sqrt{2} \quad \gamma_{yz}/\sqrt{2} \right]^T \\ \vec{s} = \left[s_x \quad s_y \quad s_z \quad \tau_{xy}\sqrt{2} \quad \tau_{xz}\sqrt{2} \quad \tau_{yz}\sqrt{2} \right]^T \\ \vec{e} = \left[e_x \quad e_y \quad e_z \quad \gamma_{xy}/\sqrt{2} \quad \gamma_{xz}/\sqrt{2} \quad \gamma_{yz}/\sqrt{2} \right]^T \end{cases} \tag{1}$$

where τ_{ij} and γ_{ij} are shear strain components, and T stands for the transpose of a vector. Voigt-Mandel's 6D notation is extensively used in solid mechanics to model stress-strain relations, particu-

larly to improve computational efficiency in numerical structural mechanics software, since it only needs six scalar variables to represent each 3×3 tensor.

The $\sqrt{2}$ terms in Voigt-Mandel's vector notation makes it geometrically equivalent to the tensor notation. The transformation from 6D stresses or strains to their deviatoric part can be represented by a 6×6 projection matrix $[A_{6D}]$ through $\vec{s} = A_{6D} \cdot \vec{\sigma}$ and $\vec{e} = A_{6D} \cdot \vec{\varepsilon}$, where

$$[A_{6D}] = \begin{bmatrix} 2/3 & -1/3 & -1/3 & 0 & 0 & 0 \\ -1/3 & 2/3 & -1/3 & 0 & 0 & 0 \\ -1/3 & -1/3 & 2/3 & 0 & 0 & 0 \\ 0 & 0 & 0 & 1 & 0 & 0 \\ 0 & 0 & 0 & 0 & 1 & 0 \\ 0 & 0 & 0 & 0 & 0 & 1 \end{bmatrix} \tag{2}$$

If $\vec{\varepsilon}$ is elastoplastic, then it is possible to represent its elastic and plastic components in Voigt-Mandel's notation through $\vec{\varepsilon} = \vec{\varepsilon}_{el} + \vec{\varepsilon}_{pl}$, where

$$\begin{aligned} \vec{\varepsilon}_{el} &= \left[\varepsilon_{x_{el}} \quad \varepsilon_{y_{el}} \quad \varepsilon_{z_{el}} \quad \gamma_{xy_{el}}/\sqrt{2} \quad \gamma_{xz_{el}}/\sqrt{2} \quad \gamma_{yz_{el}}/\sqrt{2} \right]^T \\ \vec{\varepsilon}_{pl} &= \left[\varepsilon_{x_{pl}} \quad \varepsilon_{y_{pl}} \quad \varepsilon_{z_{pl}} \quad \gamma_{xy_{pl}}/\sqrt{2} \quad \gamma_{xz_{pl}}/\sqrt{2} \quad \gamma_{yz_{pl}}/\sqrt{2} \right]^T \end{aligned} \tag{3}$$

2.2 Ilyushin deviatoric spaces

When dealing with multiaxial stress-strain calculations, it is a good idea to work in stress or strain spaces with reduced dimensions, to save computational cost without modifying the results. By working in the deviatoric space, several equations can be simplified, e.g. Hooke's law becomes a scalar operation instead of involving stiffness matrices. Voigt-Mandel's 6D *vectorial* representation of the deviatoric stresses $\vec{s}$ and strains $\vec{e}$ is a good choice, since it is geometrically equivalent to the deviatoric *tensors*, and Hooke's law only requires a scalar elastic parameter $2G$, where G is the shear elastic modulus.

As the deviatoric stresses s_x, s_y and s_z are linearly-dependent, since $s_x + s_y + s_z = 0$, it is possible to reduce the deviatoric stress space dimension from 6D to 5D, defining a 5D deviatoric stress vector $\vec{s}' = [s_1\ s_2\ s_3\ s_4\ s_5]^T$ [4]. There are infinite ways to do this, e.g. defining s_3, s_4 and s_5 as proportional to the shear stresses τ_{xy}, τ_{xz} and τ_{yz}, while representing the normal stresses σ_x, σ_y and σ_z by their hydrostatic component σ_h and two new variables s_1 and s_2, through

$$\begin{bmatrix} s_1 \\ s_2 \\ \sigma_h \end{bmatrix} = \begin{bmatrix} a_{x1} & a_{y1} & a_{z1} \\ a_{x2} & a_{y2} & a_{z2} \\ 1/3 & 1/3 & 1/3 \end{bmatrix} \cdot \begin{bmatrix} \sigma_x \\ \sigma_y \\ \sigma_z \end{bmatrix} \tag{4}$$

where the user-defined coefficients a_{x1}, a_{y1}, a_{z1}, a_{x2}, a_{y2} and a_{z2} are values that make the transformation matrix rows $[a_{x1}\ a_{y1}\ a_{z1}]$, $[a_{x2}\ a_{y2}\ a_{z2}]$, and $[1/3\ 1/3\ 1/3]$ become linearly independent.

To avoid undesirable geometric distortions in this transformation, the axes associated with s_1, s_2 and σ_h should also be orthogonal. Hence, the axes associated with the components s_1 and s_2 should be

defined on the deviatoric plane and perpendicular to each other. Using this requirement, a family of coordinate transformations involving a scaling factor k_s and a rotation angle φ_s can be proposed, see Fig. 1(left), where

$$\begin{bmatrix} s_1 \\ s_2 \end{bmatrix} = \begin{bmatrix} a_{x1} & a_{y1} & a_{z1} \\ a_{x2} & a_{y2} & a_{z2} \end{bmatrix} \cdot \begin{bmatrix} \sigma_x \\ \sigma_y \\ \sigma_z \end{bmatrix} = k_s \cdot \begin{bmatrix} \cos(\varphi_s) & \cos(\varphi_s + 120^o) & \cos(\varphi_s + 240^o) \\ \sin(\varphi_s) & \sin(\varphi_s + 120^o) & \sin(\varphi_s + 240^o) \end{bmatrix} \cdot \begin{bmatrix} \sigma_x \\ \sigma_y \\ \sigma_z \end{bmatrix} \tag{5}$$

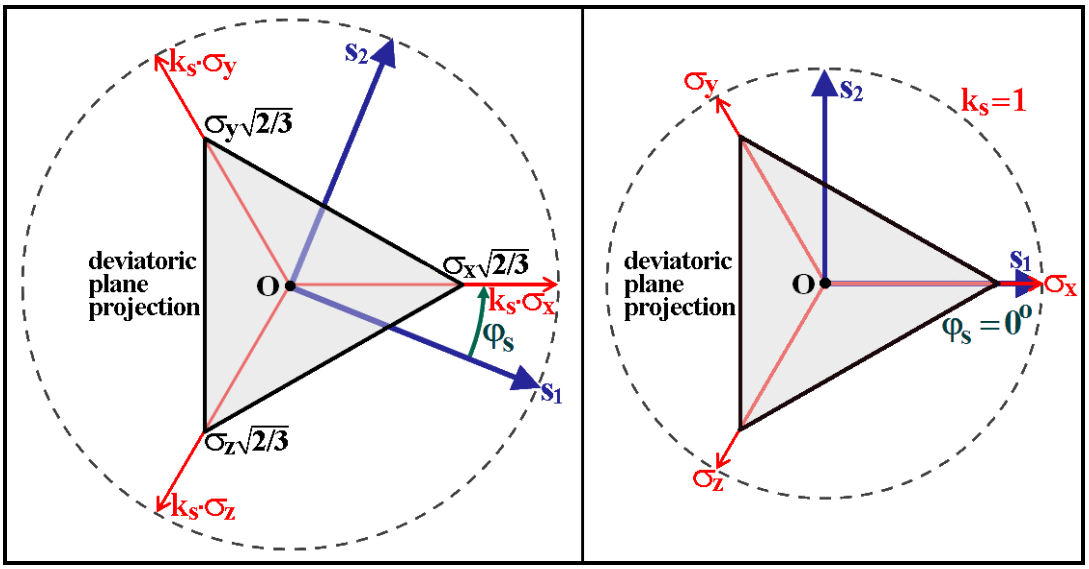

Fig. 1: Coordinate transformations between the normal stresses σ_x, σ_y and σ_z and the deviatoric stresses s_1 and s_2 on the deviatoric plane, for a generic scaling factor k_s and rotation angle φ_s (left) and for the adopted $k_s = 1$ and $\varphi_s = 0^o$ (right).

This is a generalization of the classical Ilyushin's transformations [5], which adopted the particular scaling factor $k_S = \cos 35.3^o = \sqrt{2/3}$. Defining $s_3 \equiv k_s \sqrt{3} \cdot \tau_{xy}$, $s_4 \equiv k_s \sqrt{3} \cdot \tau_{xz}$ and $s_5 \equiv k_s \sqrt{3} \cdot \tau_{yz}$, it can be shown that, for any φ_s,

$$\left.\begin{aligned} s_1^2 + s_2^2 &= k_s^2 \cdot \left(\sigma_x^2 + \sigma_y^2 + \sigma_z^2 - \sigma_x\sigma_y - \sigma_x\sigma_z - \sigma_y\sigma_z\right) \\ s_3^2 + s_4^2 + s_5^2 &\equiv k_s^2 \cdot 3\left(\tau_{xy}^2 + \tau_{xz}^2 + \tau_{yz}^2\right) \end{aligned}\right\} \Rightarrow |\vec{s}'| = \sigma_{Mises} \cdot k_s \tag{6}$$

where σ_{Mises} is the von Mises equivalent stress, and $|\,.\,|$ stands for the Euclidean norm of a vector. Note that Ilyushin's $k_S = \cos 35.3^o = \sqrt{2/3}$ makes the 6D $\vec{s}$ and the 5D $\vec{s}'$ have the same norm.

On the other hand, adopting instead $k_s = 1$ conveniently results in $|\vec{s}'| = \sigma_{Mises}$. The resulting transformation between the 5D deviatoric stress $\vec{s}'$ and the 6D stress $\vec{\sigma}$ becomes $\vec{s}' = A(k_s, \varphi_s) \cdot \vec{\sigma}$, where the projection matrix $A(k_s, \varphi_s)$ is given by:

$$\underbrace{\begin{bmatrix} s_1 \\ s_2 \\ s_3 \\ s_4 \\ s_5 \end{bmatrix}}_{\vec{s}'} = k_s \cdot \underbrace{\begin{bmatrix} \cos(\varphi_s) & \cos(\varphi_s + 120^o) & \cos(\varphi_s + 240^o) & 0 & 0 & 0 \\ \sin(\varphi_s) & \sin(\varphi_s + 120^o) & \sin(\varphi_s + 240^o) & 0 & 0 & 0 \\ 0 & 0 & 0 & \sqrt{3/2} & 0 & 0 \\ 0 & 0 & 0 & 0 & \sqrt{3/2} & 0 \\ 0 & 0 & 0 & 0 & 0 & \sqrt{3/2} \end{bmatrix}}_{A(k_S, \varphi_S)} \cdot \underbrace{\begin{bmatrix} \sigma_x \\ \sigma_y \\ \sigma_z \\ \tau_{xy}\sqrt{2} \\ \tau_{xz}\sqrt{2} \\ \tau_{yz}\sqrt{2} \end{bmatrix}}_{\vec{\sigma}} \tag{7}$$

Note that the 6D-to-5D projection matrix adopted by Papadopoulos [6] is a particular case of Eq. (7), namely for $A(k_s = 1/\sqrt{3},\ \varphi_s = 0^o)$. The 5D Euclidean sub-space E_{5s} adopted in this work uses instead a projection matrix $A(k_s = 1,\ \varphi_s = 0^o)$, see Fig. 1(right), to make its metric $|\vec{s}'|$ equal to σ_{Mises} (note that the prime in the vector notation means that it is defined in the 5D space)

$$\vec{s}' \equiv \begin{bmatrix} s_1 \\ s_2 \\ s_3 \\ s_4 \\ s_5 \end{bmatrix} = \underbrace{\begin{bmatrix} 1 & -1/2 & -1/2 & 0 & 0 & 0 \\ 0 & \sqrt{3}/2 & -\sqrt{3}/2 & 0 & 0 & 0 \\ 0 & 0 & 0 & \sqrt{3/2} & 0 & 0 \\ 0 & 0 & 0 & 0 & \sqrt{3/2} & 0 \\ 0 & 0 & 0 & 0 & 0 & \sqrt{3/2} \end{bmatrix}}_{A} \cdot \begin{bmatrix} \sigma_x \\ \sigma_y \\ \sigma_z \\ \tau_{xy}\sqrt{2} \\ \tau_{xz}\sqrt{2} \\ \tau_{yz}\sqrt{2} \end{bmatrix} \equiv A \cdot \vec{\sigma} \tag{8}$$

Such adopted transformation remains unchanged if σ_x, σ_y and σ_z are replaced respectively by their deviatoric components s_x, s_y and s_z, therefore

$$\vec{s}' \equiv \begin{bmatrix} s_1 & s_2 & s_3 & s_4 & s_5 \end{bmatrix}^T = A \cdot \vec{\sigma} = A \cdot \vec{s} \tag{9}$$

where

$$\begin{cases} s_1 \equiv \sigma_x - (\sigma_y + \sigma_z)/2 = 3s_x/2, \quad s_2 \equiv (\sigma_y - \sigma_z)\sqrt{3}/2 = (s_y - s_z)\sqrt{3}/2 \\ s_3 \equiv \tau_{xy}\sqrt{3}, \quad s_4 \equiv \tau_{xz}\sqrt{3}, \quad s_5 \equiv \tau_{yz}\sqrt{3} \end{cases} \tag{10}$$

The above defined 5D deviatoric stress vector $\vec{s}'$ has three important properties:

1. The Euclidean norm of the 5D vector $\vec{s}'$ from the E_{5s} deviatoric sub-space is equal to the Mises equivalent stress σ_{Mises}, thus

$$|\vec{s}'| = |\vec{s}|/\sqrt{2/3} = \sigma_{Mises} \equiv \tau_{Mises}\sqrt{3} \tag{11}$$

2. The Euclidean distance in the E_{5s} space between two stress states (points) A and B, defined by $\vec{s}'_A = [s_{1A}\ s_{2A}\ s_{3A}\ s_{4A}\ s_{5A}]^T$ and $\vec{s}'_B = [s_{1B}\ s_{2B}\ s_{3B}\ s_{4B}\ s_{5B}]^T$, respectively associated with the 6D deviatoric stresses $\vec{s}_A$ and $\vec{s}_B$, is equal to the Mises range $\Delta\sigma_{Mises}$ between these stress states:

$$|\vec{s}'_B - \vec{s}'_A| = |\vec{s}_B - \vec{s}_A|/\sqrt{2/3} = \Delta\sigma_{Mises} \equiv \Delta\tau_{Mises}\sqrt{3} \tag{12}$$

3. The locus of the points that have the same range $\Delta\sigma_{Mises}$ with respect to a stress state $\vec{s}'$ in E_{5s} is the surface of a hypersphere with center in $\vec{s}'$ and radius $\Delta\sigma_{Mises}$, a corollary from the second property.

Note that such properties are valid for any projection matrix with a scaling factor $k_s = 1$, independently of the choice of φ_s, i.e., for any projection matrix $A(1, \varphi_s)$.

2.3 Elastic and plastic deviatoric strain spaces

For strain histories, it is also possible to represent the deviatoric strains in 5D strain-based sub-spaces. In this work, the same $A(1, 0^o)$ projection matrix is used for strains, resulting in the 5D Euclidean sub-space E_{5e} with coordinates

$$\vec{e}' \equiv \begin{bmatrix} e_1 & e_2 & e_3 & e_4 & e_5 \end{bmatrix}^T = A \cdot \vec{\varepsilon} = A \cdot \vec{e} \tag{13}$$

where

$$\begin{cases} e_1 \equiv \varepsilon_x - \dfrac{\varepsilon_y + \varepsilon_z}{2} = \dfrac{3}{2} e_x, \;\; e_2 \equiv \dfrac{\varepsilon_y - \varepsilon_z}{2}\sqrt{3} = \dfrac{e_y - e_z}{2}\sqrt{3} \\ e_3 \equiv \dfrac{\gamma_{xy}}{2}\sqrt{3}, \;\; e_4 \equiv \dfrac{\gamma_{xz}}{2}\sqrt{3}, \;\; e_5 \equiv \dfrac{\gamma_{yz}}{2}\sqrt{3} \end{cases} \tag{14}$$

This 5D deviatoric strain $\vec{e}'$ in the defined sub-space E_{5e} also has three important properties, very similar to the E_{5s} stress sub-space properties:

1. The Euclidean norm of the 5D vector $\vec{e}'$ divided by $1+\bar{\nu}$ is equal to the Mises equivalent strain ε_{Mises}:

$$\frac{|\vec{e}'|}{1+\bar{\nu}} = \frac{1}{1+\bar{\nu}} \cdot \frac{|\vec{e}|}{\sqrt{2/3}} = \varepsilon_{Mises} \equiv \frac{1}{1+\bar{\nu}} \cdot \frac{\gamma_{Mises}}{2}\sqrt{3} \tag{15}$$

   where $\bar{\nu}$ is the effective Poisson ratio, a weighted average between the elastic ν and plastic 0.5 Poisson ratios.

2. The Euclidean distance in the E_{5e} sub-space between two points, divided by $1+\bar{\nu}$, is equal to the Mises strain range $\Delta\varepsilon_{Mises}$ between these strain states.

3. The locus of the points with same $\Delta\varepsilon_{Mises}$ with respect to a point $\vec{e}'$ in the E_{5e} sub-space is the surface of a 5D hypersphere with center in $\vec{e}'$ and radius $\Delta\varepsilon_{Mises} \cdot (1+\bar{\nu})$, a corollary from the second property.

The 5D deviatoric stresses and strains proposed above can represent any multiaxial history, even at points below the surface of the specimen. In the particular case of points on a free surface perpendicular to the *z* direction, where $\tau_{xz} = \tau_{yz} = 0$ and $\gamma_{xz} = \gamma_{yz} = 0$ but allowing $\sigma_z \neq 0$ (due e.g. to a surface pressure), the proposed deviatoric stress and strain vectors can be further reduced to 3D sub-spaces

$$\begin{cases} \vec{s}_{3D} \equiv \begin{bmatrix} s_1 & s_2 & s_3 \end{bmatrix}^T = \begin{bmatrix} \sigma_x - \dfrac{\sigma_y + \sigma_z}{2} & \dfrac{\sigma_y - \sigma_z}{2}\sqrt{3} & \tau_{xy}\sqrt{3} \end{bmatrix}^T \\ \vec{e}_{3D} \equiv \begin{bmatrix} e_1 & e_2 & e_3 \end{bmatrix}^T = \begin{bmatrix} \varepsilon_x - \dfrac{\varepsilon_y + \varepsilon_z}{2} & \dfrac{\varepsilon_y - \varepsilon_z}{2}\sqrt{3} & \dfrac{\gamma_{xy}}{2}\sqrt{3} \end{bmatrix}^T \end{cases} \tag{16}$$

Moreover, for surface histories consisting of combinations of only uniaxial tension σ_x and torsion τ_{xy}, 2D sub-spaces could be used to simplify even further the representation of the deviatoric stress and strain vectors

$$\begin{cases} \vec{s}_{2D} \equiv \begin{bmatrix} s_1 & s_3 \end{bmatrix}^T = \begin{bmatrix} \sigma_x & \tau_{xy}\sqrt{3} \end{bmatrix}^T \\ \vec{e}_{2D} \equiv \begin{bmatrix} e_1 & e_3 \end{bmatrix}^T = \begin{bmatrix} \varepsilon_x \cdot (1+\bar{\nu}) & \dfrac{\gamma_{xy}}{2}\sqrt{3} \end{bmatrix}^T \end{cases} \tag{17}$$

Such simplifications are a major advantage of the E_{5s} and E_{5e} spaces. For instance, since the stress component σ_x shows up in all deviatoric components s_x, s_y and s_z, a simple tension-torsion history would normally need to be represented in a 4D sub-space $\left[s_x \;\; s_y \;\; s_z \;\; \tau_{xy}\sqrt{2} \right]^T$ if Voigt-Mandel's notation was used, instead of the above reduced 2D formulation. Note that, for uniaxial histories, the trivial scalar sub-spaces $\vec{s}_{1D} \equiv \left[s_1 \right]$ and $\vec{e}_{1D} \equiv \left[e_1 \right]$ could be adopted.

Instead of having to deal with the effective Poisson ratio $\bar{\nu}$, which is an approximation combining the elastic ν and plastic *0.5* Poisson ratios, it is much better to represent the deviatoric strain as a sum of its elastic and plastic components $\vec{e}' = \vec{e}_{el} + \vec{e}_{pl}$ in 5D:

$$\vec{e}'_{el} \equiv \left[e_{1_{el}} \;\; e_{2_{el}} \;\; e_{3_{el}} \;\; e_{4_{el}} \;\; e_{5_{el}} \right]^T = A \cdot \vec{\varepsilon}_{el} = A \cdot \vec{e}_{el} \tag{18}$$

$$\vec{e}'_{pl} \equiv \left[e_{1_{pl}} \;\; e_{2_{pl}} \;\; e_{3_{pl}} \;\; e_{4_{pl}} \;\; e_{5_{pl}} \right]^T = A \cdot \vec{\varepsilon}_{pl} = A \cdot \vec{e}_{pl} \tag{19}$$

where *el* and *pl* subscripts stand respectively for elastic and plastic components, and

$$\begin{cases} e_{1_{el}} \equiv \varepsilon_{x_{el}} - \dfrac{\varepsilon_{y_{el}} + \varepsilon_{z_{el}}}{2} = \dfrac{3}{2} e_{x_{el}}, \quad e_{2_{el}} \equiv \dfrac{\varepsilon_{y_{el}} - \varepsilon_{z_{el}}}{2}\sqrt{3} = \dfrac{e_{y_{el}} - e_{z_{el}}}{2}\sqrt{3} \\ e_{3_{el}} \equiv \dfrac{\gamma_{xy_{el}}}{2}\sqrt{3}, \quad e_{4_{el}} \equiv \dfrac{\gamma_{xz_{el}}}{2}\sqrt{3}, \quad e_{5_{el}} \equiv \dfrac{\gamma_{yz_{el}}}{2}\sqrt{3} \end{cases} \tag{20}$$

$$\begin{cases} e_{1_{pl}} \equiv \varepsilon_{x_{pl}} - \dfrac{\varepsilon_{y_{pl}} + \varepsilon_{z_{pl}}}{2} = \dfrac{3}{2} e_{x_{pl}}, \quad e_{2_{pl}} \equiv \dfrac{\varepsilon_{y_{pl}} - \varepsilon_{z_{pl}}}{2}\sqrt{3} = \dfrac{e_{y_{pl}} - e_{z_{pl}}}{2}\sqrt{3} \\ e_{3_{pl}} \equiv \dfrac{\gamma_{xy_{pl}}}{2}\sqrt{3}, \quad e_{4_{pl}} \equiv \dfrac{\gamma_{xz_{pl}}}{2}\sqrt{3}, \quad e_{5_{pl}} \equiv \dfrac{\gamma_{yz_{pl}}}{2}\sqrt{3} \end{cases} \tag{21}$$

The 5D plastic strain space defined by $\vec{e}'_{pl}$ is hereby called E_{5p} space. Note that such $\vec{e}'_{pl}$ vector, multiplied by *3/2*, is identical to the 5D representation of plastic strains proposed by Tanaka [7]:

$$\vec{e}'_{pl} = \frac{3}{2} \cdot \underbrace{\left[e_{x_{pl}} \;\; \frac{e_{x_{pl}} + 2e_{y_{pl}}}{\sqrt{3}} \;\; \frac{\gamma_{xy_{pl}}}{\sqrt{3}} \;\; \frac{\gamma_{xz_{pl}}}{\sqrt{3}} \;\; \frac{\gamma_{yz_{pl}}}{\sqrt{3}} \right]^T}_{\textit{Tanaka's 5D deviatoric space}} \tag{22}$$

since the identity $e_{xpl} + e_{ypl} + e_{zpl} = 0$ implies that $e_{ypl} - e_{zpl} = e_{xpl} + 2e_{ypl}$. Therefore, Tanaka's efficient non-proportional hardening model [7] can be directly computed in the proposed E_{5p} formulation, without requiring any additional plastic strain projection.

Similarly to the E_{5s} stress sub-space, 3D and 2D versions of the strain spaces can also be defined respectively under free-surface and tension-torsion conditions, resulting in

$$\begin{cases} \vec{e}_{3D_{el}} \equiv \left[\varepsilon_{x_{el}} - \dfrac{\varepsilon_{y_{el}} + \varepsilon_{z_{el}}}{2} \;\; \dfrac{\varepsilon_{y_{el}} - \varepsilon_{z_{el}}}{2}\sqrt{3} \;\; \dfrac{\gamma_{xy_{el}}}{2}\sqrt{3} \right]^T \\ \vec{e}_{3D_{pl}} \equiv \dfrac{3}{2} \cdot \left[\varepsilon_{x_{pl}} \;\; \dfrac{\varepsilon_{y_{pl}} - \varepsilon_{z_{pl}}}{\sqrt{3}} \;\; \dfrac{\gamma_{xy_{pl}}}{\sqrt{3}} \right]^T \end{cases} \tag{23}$$

$$\begin{cases} \vec{e}_{2D_{el}} \equiv (1+\nu)\cdot\left[\varepsilon_{x_{el}} \quad \dfrac{\gamma_{xy_{el}}}{2\cdot(1+\nu)}\sqrt{3}\right]^T \\ \vec{e}_{2D_{pl}} \equiv \dfrac{3}{2}\cdot\left[\varepsilon_{x_{pl}} \quad \dfrac{\gamma_{xy_{pl}}}{\sqrt{3}}\right]^T \end{cases} \tag{24}$$

Note that the plastic 2D sub-space where $\vec{e}_{2D_{pl}}$ is represented is equivalent to the classic Mises diagram $\varepsilon_{xpl} \times \gamma_{xypl}/\sqrt{3}$ multiplied by *3/2*. But the common practice of representing the elastoplastic strain history in tension-torsion tests using an $\varepsilon_x \times \gamma_{xy}/\sqrt{3}$ diagram is only appropriate if plastic strains dominate, i.e. if $\varepsilon_x \cong \varepsilon_{xpl}$, $\gamma_{xy} \cong \gamma_{xypl}$ and thus $\vec{e}_{2D} \cong \vec{e}_{2D_{pl}}$. Otherwise, $\vec{e}_{2Del}$ and $\vec{e}_{2D_{pl}}$ should be studied in separate elastic and plastic diagrams, or altogether in a single elastoplastic diagram $\vec{e}_{2D}$ using the effective Poisson ratio.

2.4 Direct and inverse transforms between the adopted 6D and 5D spaces

The inverse transform from the 5D to the 6D space is now calculated using the projection matrix *A* defined in Eq. (8). Two important properties of *A* are $A\cdot A^T = 1.5\cdot I_{5\times5}$ and $A^T\cdot A = 1.5\cdot A_{6D}$, where $I_{5\times5}$ is the 5×5 identity matrix and A_{6D} is the projection matrix onto the 6D deviatoric space in Voigt-Mandel's notation, shown in Eq. (2). These identities would also be valid for any other projection matrix $A(k_s = 1, \varphi_s)$, independently of the orientation φ_s of the chosen s_1-s_2 coordinate frame. However, *A* is a 5×6 matrix, thus it cannot be inverted since it is not square. But its *right pseudo-inverse* could be used instead.

The *right pseudo-inverse* of a matrix *X*, defined as $pinv(X) \equiv X^T\cdot(X\cdot X^T)^{-1}$, is a generalization of the inverse that is valid even for non-square matrices. If $X\cdot X^T$ is invertible, then it is easy to show that $X\cdot pinv(X) = (X\cdot X^T)\cdot(X\cdot X^T)^{-1}$ is equal to the identity matrix, analogously to the properties of a square inverse matrix. The *right pseudo-inverse* of *A* becomes then

$$pinv(A) \equiv A^T\cdot(A\cdot A^T)^{-1} = A^T\cdot(1.5\cdot I_{5\times5})^{-1} = 1.5\cdot A^T \tag{25}$$

which can be used to calculate the inverse transform from the considered 5D stress sub-space back to 6D. But, even though $\vec{s}' = A\cdot\vec{\sigma}$, in general it is not true that $pinv(A)\cdot\vec{s}'$ is equal to the original 6D stress $\vec{\sigma}$. Instead, this product results in the 6D deviatoric stress $\vec{s}$

$$pinv(A)\cdot\vec{s}' = \frac{2}{3}A^T\cdot(A\cdot\vec{\sigma}) = \frac{2}{3}\cdot\frac{3}{2}A_{6D}\cdot\vec{\sigma} = \vec{s} \Rightarrow \vec{s} = pinv(A)\cdot\vec{s}' \tag{26}$$

The reconstruction of the 6D $\vec{\sigma}$ would also require the knowledge of the 6D hydrostatic stress vector $\vec{\sigma}_h = \sigma_h\cdot[1 \;\; 1 \;\; 1 \;\; 0 \;\; 0 \;\; 0]^T$ to obtain $\vec{\sigma} = \vec{s} + \vec{\sigma}_h$. In an analogous way as done for stresses, the pseudo-inverse can also be used to project 5D strains back to their 6D space. The direct and inverse transformations using the proposed projection matrix *A* are summarized in Tables 1 and 2.

Table 1: Direct and inverse matrix transforms between Voigt-Mandel's 6D and the proposed 5D spaces, where $A \cdot A^T = 1.5 \cdot I_{5\times5}$ and $A^T \cdot A = 1.5 \cdot A_{6D}$.

transform	*From 6D to 5D*	*From 5D to 6D*
stress	$\vec{\mathbf{s}}' = \mathbf{A}\cdot\vec{\boldsymbol{\sigma}} = \mathbf{A}\cdot\vec{\mathbf{s}} = \mathbf{A}'\cdot\vec{\mathbf{s}}$	$\vec{\mathbf{s}} = (2/3)\,\mathbf{A}^{\mathbf{T}}\cdot\vec{\mathbf{s}}' \;\Rightarrow\; \vec{\boldsymbol{\sigma}} = \vec{\mathbf{s}} + \vec{\boldsymbol{\sigma}}_{\mathbf{h}}$
elastoplastic strain	$\vec{\mathbf{e}}' = \mathbf{A}\cdot\vec{\boldsymbol{\varepsilon}} = \mathbf{A}\cdot\vec{\mathbf{e}}$	$\vec{\mathbf{e}} = (2/3)\,\mathbf{A}^{\mathbf{T}}\cdot\vec{\mathbf{e}}' \;\Rightarrow\; \vec{\boldsymbol{\varepsilon}} = \vec{\mathbf{e}} + \vec{\boldsymbol{\varepsilon}}_{\mathbf{h}}$
elastic strain	$\vec{\mathbf{e}}'_{\mathbf{el}} = \mathbf{A}\cdot\vec{\boldsymbol{\varepsilon}}_{\mathbf{el}} = \mathbf{A}\cdot\vec{\mathbf{e}}_{\mathbf{el}}$	$\vec{\mathbf{e}}_{\mathbf{el}} = (2/3)\,\mathbf{A}^{\mathbf{T}}\cdot\vec{\mathbf{e}}'_{\mathbf{el}} \;\Rightarrow\; \vec{\boldsymbol{\varepsilon}}_{\mathbf{el}} = \vec{\mathbf{e}}_{\mathbf{el}} + \vec{\boldsymbol{\varepsilon}}_{\mathbf{h}}$
plastic strain	$\vec{\mathbf{e}}'_{\mathbf{pl}} = \mathbf{A}\cdot\vec{\boldsymbol{\varepsilon}}_{\mathbf{pl}} = \mathbf{A}\cdot\vec{\mathbf{e}}_{\mathbf{pl}}$	$\vec{\mathbf{e}}_{\mathbf{pl}} = \vec{\mathbf{e}}'_{\mathbf{pl}} = (2/3)\,\mathbf{A}^{\mathbf{T}}\cdot\vec{\mathbf{e}}'_{\mathbf{pl}}$ (since $\vec{\boldsymbol{\varepsilon}}_{\mathbf{h}}$ is elastic)

Table 2: Direct and inverse scalar transformations between the 6D and 5D representations.

transform	*From 6D to 5D*	*From 5D to 6D*
stress	$\mathbf{s_1} = \boldsymbol{\sigma}_\mathbf{x} - (\boldsymbol{\sigma}_\mathbf{y} + \boldsymbol{\sigma}_\mathbf{z})/2$ $\mathbf{s_2} = (\boldsymbol{\sigma}_\mathbf{y} - \boldsymbol{\sigma}_\mathbf{z})\sqrt{3}/2$ $\mathbf{s_3} = \boldsymbol{\tau}_{\mathbf{xy}}\sqrt{3},\ \mathbf{s_4} = \boldsymbol{\tau}_{\mathbf{xz}}\sqrt{3}$ $\mathbf{s_5} = \boldsymbol{\tau}_{\mathbf{yz}}\sqrt{3}$	$\boldsymbol{\sigma}_\mathbf{x} = \boldsymbol{\sigma}_\mathbf{h} + \mathbf{s_1}\cdot 2/3$ $\boldsymbol{\sigma}_\mathbf{y} = \boldsymbol{\sigma}_\mathbf{h} - \mathbf{s_1}/3 + \mathbf{s_2}/\sqrt{3}$ $\boldsymbol{\sigma}_\mathbf{z} = \boldsymbol{\sigma}_\mathbf{h} - \mathbf{s_1}/3 - \mathbf{s_2}/\sqrt{3}$ $\boldsymbol{\tau}_{\mathbf{xy}} = \mathbf{s_3}/\sqrt{3},\ \boldsymbol{\tau}_{\mathbf{xz}} = \mathbf{s_4}/\sqrt{3},\ \boldsymbol{\tau}_{\mathbf{yz}} = \mathbf{s_5}/\sqrt{3}$
elastoplastic strain	$\mathbf{e_1} = \boldsymbol{\varepsilon}_\mathbf{x} - (\boldsymbol{\varepsilon}_\mathbf{y} + \boldsymbol{\varepsilon}_\mathbf{z})/2$ $\mathbf{e_2} = (\boldsymbol{\varepsilon}_\mathbf{y} - \boldsymbol{\varepsilon}_\mathbf{z})\sqrt{3}/2$ $\mathbf{e_3} = \boldsymbol{\gamma}_{\mathbf{xy}}\sqrt{3}/2$ $\mathbf{e_4} = \boldsymbol{\gamma}_{\mathbf{xz}}\sqrt{3}/2$ $\mathbf{e_5} = \boldsymbol{\gamma}_{\mathbf{yz}}\sqrt{3}/2$	$\boldsymbol{\varepsilon}_\mathbf{x} = \boldsymbol{\varepsilon}_\mathbf{h} + \mathbf{e_1}\cdot 2/3$ $\boldsymbol{\varepsilon}_\mathbf{y} = \boldsymbol{\varepsilon}_\mathbf{h} - \mathbf{e_1}/3 + \mathbf{e_2}/\sqrt{3}$ $\boldsymbol{\varepsilon}_\mathbf{z} = \boldsymbol{\varepsilon}_\mathbf{h} - \mathbf{e_1}/3 - \mathbf{e_2}/\sqrt{3}$ $\boldsymbol{\gamma}_{\mathbf{xy}} = \mathbf{e_3}\cdot 2/\sqrt{3},\ \ \boldsymbol{\gamma}_{\mathbf{xz}} = \mathbf{e_4}\cdot 2/\sqrt{3}$ $\boldsymbol{\gamma}_{\mathbf{yz}} = \mathbf{e_5}\cdot 2/\sqrt{3}$
elastic strain	$\mathbf{e_{1_{el}}} = \boldsymbol{\varepsilon}_{\mathbf{x_{el}}} - (\boldsymbol{\varepsilon}_{\mathbf{y_{el}}} + \boldsymbol{\varepsilon}_{\mathbf{z_{el}}})/2$ $\mathbf{e_{2_{el}}} = (\boldsymbol{\varepsilon}_{\mathbf{y_{el}}} - \boldsymbol{\varepsilon}_{\mathbf{z_{el}}})\sqrt{3}/2$ $\mathbf{e_{3_{el}}} = \boldsymbol{\gamma}_{\mathbf{xy_{el}}}\sqrt{3}/2$ $\mathbf{e_{4_{el}}} = \boldsymbol{\gamma}_{\mathbf{xz_{el}}}\sqrt{3}/2$ $\mathbf{e_{5_{el}}} = \boldsymbol{\gamma}_{\mathbf{yz_{el}}}\sqrt{3}/2$	$\boldsymbol{\varepsilon}_{\mathbf{x_{el}}} = \boldsymbol{\varepsilon}_\mathbf{h} + \mathbf{e_{1_{el}}}\cdot 2/3$ $\boldsymbol{\varepsilon}_{\mathbf{y_{el}}} = \boldsymbol{\varepsilon}_\mathbf{h} - \mathbf{e_{1_{el}}}/3 + \mathbf{e_{2_{el}}}/\sqrt{3}$ $\boldsymbol{\varepsilon}_{\mathbf{z_{el}}} = \boldsymbol{\varepsilon}_\mathbf{h} - \mathbf{e_{1_{el}}}/3 - \mathbf{e_{2_{el}}}/\sqrt{3}$ $\boldsymbol{\gamma}_{\mathbf{xy_{el}}} = \mathbf{e_{3_{el}}}\cdot 2/\sqrt{3},\ \ \boldsymbol{\gamma}_{\mathbf{xz_{el}}} = \mathbf{e_{4_{el}}}\cdot 2/\sqrt{3}$ $\boldsymbol{\gamma}_{\mathbf{yz_{el}}} = \mathbf{e_{5_{el}}}\cdot 2/\sqrt{3}$
plastic strain	$\mathbf{e_{1_{pl}}} = \boldsymbol{\varepsilon}_{\mathbf{x_{pl}}} - (\boldsymbol{\varepsilon}_{\mathbf{y_{pl}}} + \boldsymbol{\varepsilon}_{\mathbf{z_{pl}}})/2$ $\mathbf{e_{2_{pl}}} = (\boldsymbol{\varepsilon}_{\mathbf{y_{pl}}} - \boldsymbol{\varepsilon}_{\mathbf{z_{pl}}})\cdot\sqrt{3}/2$ $\mathbf{e_{3_{pl}}} = \boldsymbol{\gamma}_{\mathbf{xy_{pl}}}\cdot\sqrt{3}/2$ $\mathbf{e_{4_{pl}}} = \boldsymbol{\gamma}_{\mathbf{xz_{pl}}}\cdot\sqrt{3}/2$ $\mathbf{e_{5_{pl}}} = \boldsymbol{\gamma}_{\mathbf{yz_{pl}}}\cdot\sqrt{3}/2$	$\boldsymbol{\varepsilon}_{\mathbf{x_{pl}}} = \mathbf{e_{1_{pl}}}\cdot 2/3$ $\boldsymbol{\varepsilon}_{\mathbf{y_{pl}}} = -\mathbf{e_{1_{pl}}}/3 + \mathbf{e_{2_{pl}}}/\sqrt{3}$ $\boldsymbol{\varepsilon}_{\mathbf{z_{pl}}} = -\mathbf{e_{1_{pl}}}/3 - \mathbf{e_{2_{pl}}}/\sqrt{3}$ $\boldsymbol{\gamma}_{\mathbf{xy_{pl}}} = \mathbf{e_{3_{pl}}}\cdot 2/\sqrt{3},\ \ \boldsymbol{\gamma}_{\mathbf{xz_{pl}}} = \mathbf{e_{4_{pl}}}\cdot 2/\sqrt{3}$ $\boldsymbol{\gamma}_{\mathbf{yz_{pl}}} = \mathbf{e_{5_{pl}}}\cdot 2/\sqrt{3}$

In summary, the 5D representation of stresses and strains is highly recommended, since it reduces the dimensionality of the stress-strain relations from 6D to 5D. For either free-surface conditions, un-notched tension-torsion, or uniaxial histories, respectively 3D, 2D, or 1D sub-spaces of the 5D repre-

sentation can be used, significantly decreasing computational cost. Recall that, even for a uniaxial history in *x*, Voigt-Mandel's 6D deviatoric representation would need to use three dimensions due to its redundant formulation, since σ_x is present in all three normal deviatoric components s_x, s_y and s_z. On the other hand, with a uniaxial σ_x present only in the s_1 expression, the 5D representation could use a single component in this case without problems.

The proposed 5D stress and strain formulation will be used in Part II of this paper to better describe non-linear incremental plasticity models, which are required for predicting ratcheting and mean stress relaxation effects. Such effects are discussed next, in the light of the proposed 5D formulation.

3. Uniaxial Ratcheting Behavior and Definitions

Uniaxial unbalanced histories are essentially cyclic histories with a significant mean stress component. Such histories may present plastic strain accumulation in the direction of the mean stress, called uniaxial ratcheting. Uniaxial ratcheting is a result of a different non-linear behavior of the material in tension and in compression, i.e. anisotropy between tension and compression. Masing [8] assumed that the elastoplastic hysteresis loop curves should be geometrically similar to the cyclic stress-strain curves magnified by a scale factor of two, implying that cyclically-stabilized constant-amplitude elastoplastic loops should always close. Uniaxial ratcheting behavior, however, is one in which the steady-state of a cyclic uniaxial loading is an elastoplastic loop that does not close, causing the material to accumulate a net strain during each cycle. From a microscopic point of view, this non-Masing behavior indicates an unstable microstructure in the fatigue process.

Consider the uniaxial load history shown in Fig. 2, with stresses varying between a peak $\vec{s}_{1D} = [\sigma_{max}]$ ($\sigma_{max} > S_{Yc}$) and a valley $\vec{s}_{1D} = [-S_{Yc}]$, where S_{Yc} is the cyclically-stabilized yield strength. For simplicity, the material stress-strain behavior is assumed bi-linear and without any isotropic hardening transient. The stress levels reproduced in Fig. 2 are compatible with kinematic hardening, where yielding in the opposite direction occurs after a stress variation $\Delta\sigma_x = \pm 2S_{Yc}$, but the hysteresis loops do not close. This is caused by a non-Masing behavior, where plastic straining along the path AB is larger than in CD, even though both paths are subjected to the same stress variation. This non-Masing asymmetrical behavior causes the slope of the tension path AB to be lower than the slope of the compression path CD, resulting in a net increase in plastic strain after each loop. Note that such increase in plastic strain levels cannot be explained by isotropic softening, since all paths AB, A'B' and A"B" are parallel, representing a stabilized strain hardening/softening behavior. Similarly, paths CD, C'D' and C"D" are also parallel, even though they are not parallel to AB due to the non-Masing behavior.

Since isotropic softening under stress control can also cause a net increase in plastic strain per loading cycle, it is useful to separate ratcheting from isotropic softening effects by defining the ratcheting strain as the mean strain along each cycle. In Fig. 2, the ratcheting strain ε_{ri} is thus defined after the first cycle as $\varepsilon_{r1} = (\varepsilon_B + \varepsilon_D)/2$, after the second cycle as $\varepsilon_{r2} = (\varepsilon_{B'} + \varepsilon_{D'})/2$, after the third cycle as $\varepsilon_{r3} = (\varepsilon_{B''} + \varepsilon_{D''})/2$, and so on. The ratcheting rate per cycle is then the difference $d\varepsilon/dN = (\varepsilon_{ri+1} - \varepsilon_{ri})$ between the ratcheting strains from consecutive cycles.

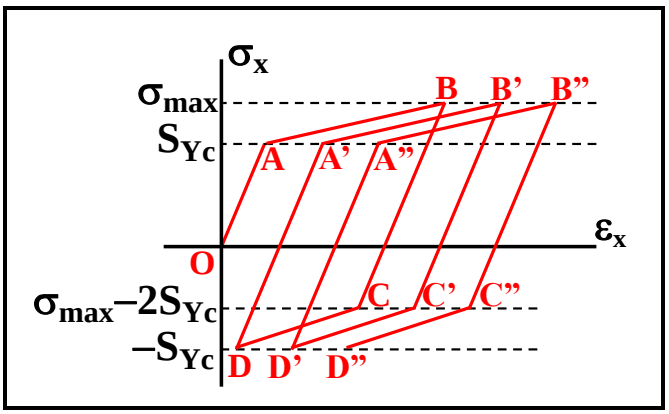

Fig. 2: Uniaxial ratcheting for a bi-linear material subjected to an unbalanced stress history between $\sigma_{max} > S_{Yc}$ and $-S_{Yc}$, under stress control, in the absence of strain hardening or softening.

This definition of the ratcheting rate is able to account only for the non-Masing asymmetrical behavior. It is independent of any isotropic transient, since isotropic hardening or softening in fully-reversed (zero mean stress) tension-compression under stress control would result in zero mean strains, therefore $\varepsilon_{ri} = 0$ and thus $d\varepsilon/dN = 0$, even though there is an increase (or decrease) of the maximum strain per cycle due to cyclic softening (or hardening, respectively).

In summary, cyclic softening and ratcheting are two different processes, the first caused by a symmetrical softening behavior in both tension and compression, and the second by a tension-compression asymmetry in the stress-strain behavior that may happen even after the strain hardening/softening transient. Both effects should be separately modeled to independently predict their similar capability to cause a net increase in plastic strain per loading cycle, even though sometimes their effects are shown superposed in the literature and simply called a ratcheting process.

The ratcheting rate $d\varepsilon/dN$ may increase with both the stress range and the mean stress [9], however it is normally much more sensitive to the mean stress [10]. The ratcheting rate usually varies with the number of cycles, even for constant amplitude loadings. For high stress ranges, the ratcheting rate $d\varepsilon/dN$ tends to increase at each cycle, until the component fails due to exhaustion of the material ductility, see Fig. 3(a). For lower stress ranges, the ratcheting rate tends to decrease until reaching steady-state with $d\varepsilon/dN = 0$, associated with a stable hysteresis loop that fully closes, see Fig. 3(b). Note also that uniaxial ratcheting may induce a significant increase in dislocation density when compared to zero-mean-strain low-cycle fatigue loading, which can cause an additional strain-hardening in certain materials, as reported in [11].

4. Multiaxial Ratcheting Analysis using Deviatoric Spaces

Multiaxial load histories can also result in gradual plastic strain accumulation along a certain direction, a phenomenon called multiaxial ratcheting, which can happen for unbalanced histories even if the material follows the Masing behavior, without any asymmetry in the hysteresis loops under tension and compression. The most common multiaxial ratcheting example can be seen in Fig. 4, which shows an elastoplastic cyclic torsion history with amplitude τ_a applied to a shaft, combined with a constant axial stress σ_m (a static "mean" stress). This example can adopt a 2D sub-space of the defined E_{5s} space, representing stress states in an $s_1 \times s_3$ diagram from the 2D vector $\vec{s}_{2D}$ defined in Eq. (17).

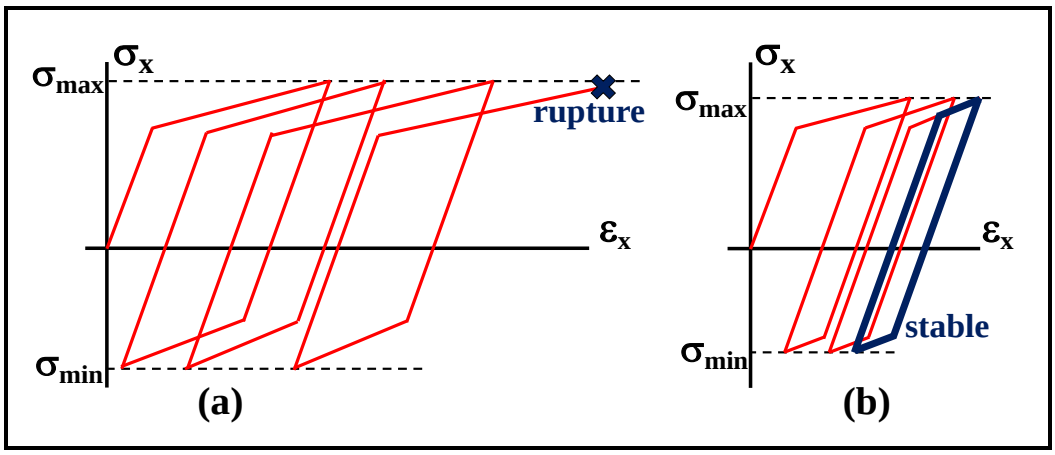

Fig. 3: Uniaxial ratcheting for a bi-linear material subjected to an unbalanced stress-controlled history under (a) high stress ranges; (b) low stress ranges.

Initially, the uniaxial path *OO'* causes elastic straining in the normal direction $[s_1 \;\; 0]^T$ until σ_m is reached, in a linear elastic process inside the yield surface. The yield surface is the locus of all points associated with a yielding criterion, which in this example is a circle since it is defined from the Mises criterion $|\vec{s}_{2D}|=S$, where *S* is the monotonic or cyclic yield strength. Since the path $O'A_0$ is inside the yield surface, it will cause an elastic shear strain, but without any axial component.

After the stress state reaches the initial yield surface at point A_0, the yield surface starts translating towards point *A*, during which plastic straining occurs. In most materials, such plastic straining happens along a direction $\vec{n}_A$ normal to the yield surface, what is known as the normality condition or normality rule, discussed in detail in Part II of this work. Since the normal vector $\vec{n}_A$ is not vertical in the example from Fig. 4(a), plastic straining along the path A_0A will not only induce an elastoplastic shear level γ_a, but it will also cause a purely plastic tensile strain increment (the ratcheting increment), where the resulting strain path describes a slope in the $\varepsilon_x \times \gamma_{xy}/\sqrt{3}$ diagram approximately equal to the slope of $\vec{n}_A$.

The path A_0A causes the yield surface to translate until its center (the backstress) reaches the position $\vec{\beta}_{2D} = [0 \;\; \beta_3]^T$ in the 2D sub-space shown in Fig. 4(b), where β_3 is the torsional component of the backstress vector in this $s_1 \times s_3$ diagram. Elastic unloading of the shear component follows along the path AB_1, until the stress state reaches the translated surface at B_1, associated with a normal vector $\vec{n}_B$. Then, the yield surface starts translating towards point *B*, causing plastic straining in both shear and axial components, along a direction in the $\varepsilon_x \times \gamma_{xy}/\sqrt{3}$ diagram approximately equal to the direction of $\vec{n}_B$, see Fig. 4(b).

Figure 4(c) shows the translated yield surface after the stress state reaches *B*, with center at a new backstress $\vec{\beta}_{2D} = [0 \;\; \beta_3]^T$ with $\beta_3 < 0$. Elastic loading follows along the path BA_1, until reaching again the yield surface at point A_1. Yielding along the path A_1A causes once again ratcheting, associated with the slope $\vec{n}_A$. The process continues, resulting in this example in a constant ratcheting rate, see Fig. 4(c). Note that yielding occurs at point A_0 only in the first cycle, while in all subsequent cycles it will happen at the A_1 stress state due to the kinematic hardening process.

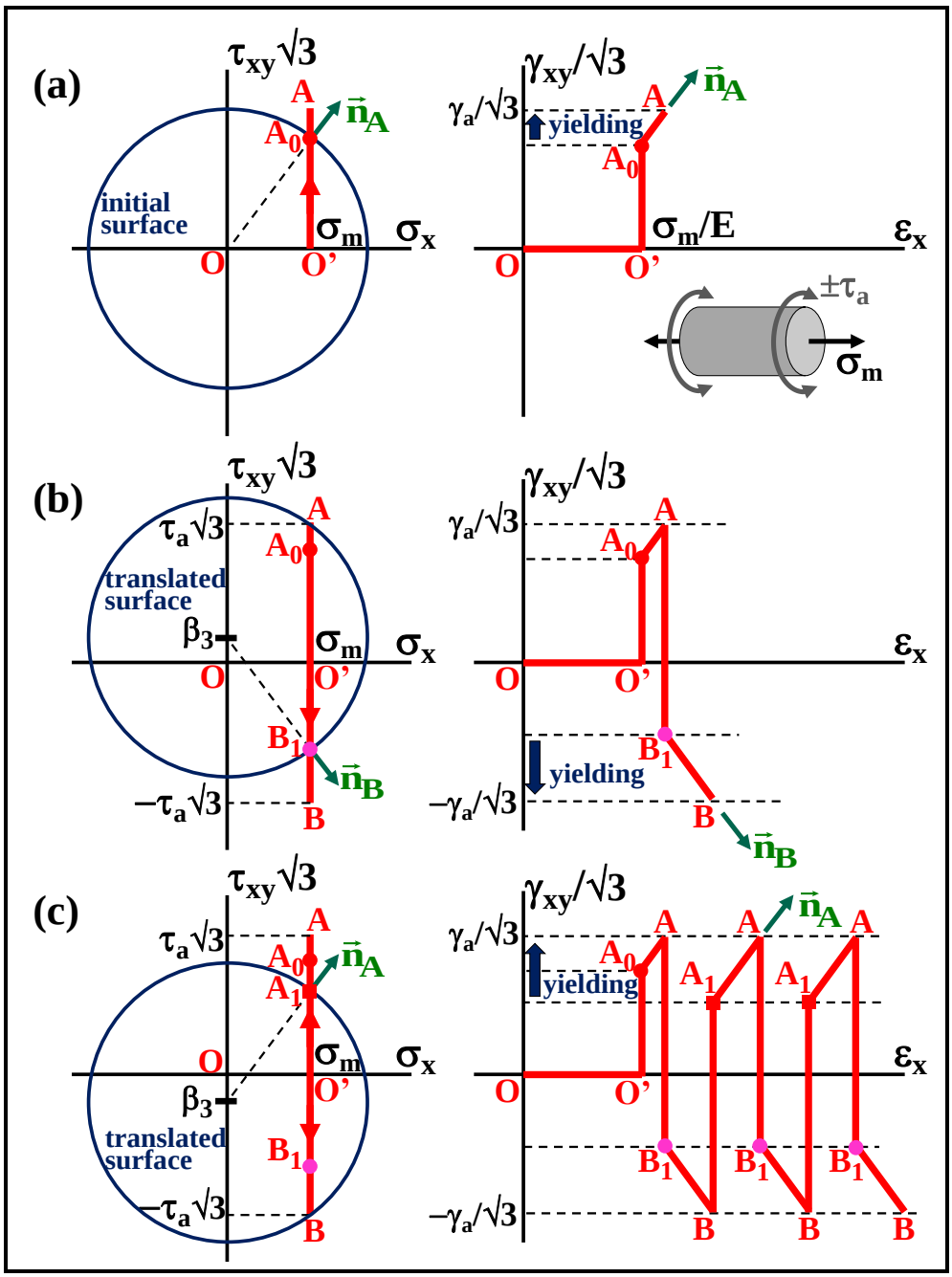

Fig. 4: Cyclic torsion history with shear amplitude τ_a and constant axial stress σ_m applied to a shaft, defined by the path *ABA* in the $\vec{s}_{2D}$ diagram $\sigma_x \times \tau_{xy}\sqrt{3}$, and resulting multiaxial ratcheting in the axial direction of the $\varepsilon_x \times \gamma_{xy}/\sqrt{3}$ diagram.

In this example, yield surface translations were all assumed in the vertical (shear) direction. However, the surface translation direction in most materials is a function of the directions of the normal vectors $\vec{n}_A$ or $\vec{n}_B$ and of the backstress vector $\vec{\beta}$, as it will be detailed in Part II of this work. The actual surface translation direction ends up changing the directions of $\vec{n}_A$ and $\vec{n}_B$ in the subsequent cycles, which in turn will change the translation direction, in a highly-coupled plasticity process. When improved surface translation equations are used to model these effects, it is found that the ratcheting rate may vary from cycle to cycle instead of being constant.

Ratcheting can also be an important problem in pressure vessels or pressurized pipelines that suffer additional cyclic shear, tension, or bending loads. Internal pressure causes a hoop stress σ_θ that acts

as the mean component associated with ratcheting problems. If the combination of σ_θ with the cyclic shear, tension, or bending stresses causes cyclic yielding, then ratcheting may occur in the hoop direction after each loading cycle, causing the vessel pipe to radially expand until eventually exhausting its ductility. Increasing ovalization of the cross section may also happen under cyclic bending, since the vessel/pipe walls will only suffer ratcheting in the highly stressed regions farther away from the neutral bending axis.

In the tension-torsion shaft example, the stress state and the yield surface were represented in the usual diagram $s_1 \times s_3 \equiv \sigma_x \times \tau_{xy}\sqrt{3}$, a sub-space of the E_{5s} stress space, since there were no other normal (or shear) components σ_y or σ_z. However, for representing cyclic tension or bending problems on a pressurized vessel/pipe, which involve three normal components σ_x, σ_θ, and σ_z acting on the inner walls, another sub-space of E_{5s} needs to be used instead, the stress diagram $s_1 \times s_2$ defined by the deviatoric components $s_1 \equiv \sigma_x - (\sigma_\theta + \sigma_z)/2$ and $s_2 \equiv (\sigma_\theta - \sigma_z)/2$, where $\sigma_z = -p$ accounts for the compressive stresses on such inner walls under a pressure $p > 0$. Even though a different sub-space of the E_{5s} stress space would be adopted, a behavior very similar to the one illustrated in Fig. 4 could be obtained. The use of the 5D formulation or its sub-spaces makes it systematic to predict ratcheting effects, with the ability to consider altogether all 6D stress or strain components, as long as a proper kinematic hardening model is adopted [12-13], as studied in Part II of this work.

5. Mean Stress Relaxation under Strain Control

Mean stress relaxation can happen during strain-controlled deformation with an initial mean stress [14], a phenomenon closely related to ratcheting. The mean stress gradually relaxes towards zero, both in uniaxial and multiaxial unbalanced histories. Consider the strain-controlled uniaxial history shown in Fig. 5, applied to the same bi-linear material from Figs. 2-4, without isotropic hardening transients. Non-Masing behavior causes the slope of paths AB, A'B' and A"B" to be smaller than the slopes of CD, C'D' and C"D", resulting in an asymmetrical behavior with open hysteresis loops that gradually decrease the mean stress component. As the mean stress tends towards zero, the non-Masing behavior diminishes, making the hysteresis loops become once again symmetric and closed.

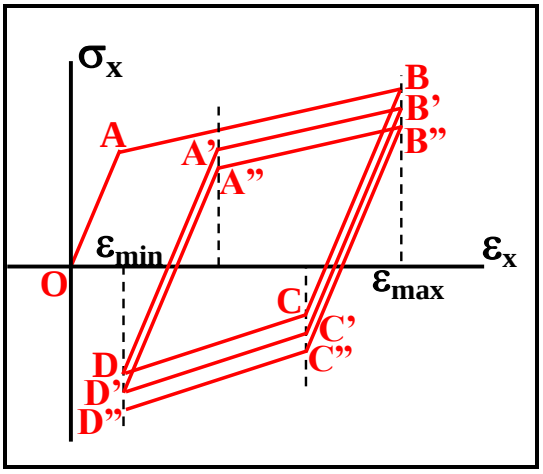

Fig. 5: Uniaxial mean stress relaxation for a bi-linear material subjected to an unbalanced strain history between ε_{min} and ε_{max}, under strain control.

Mean stress relaxation caused by high plastic strain ranges is one of the reasons why low-cycle fatigue lives are less influenced by the mean stress effect than high-cycle fatigue lives. It can also explain why the mean stress correction in the plastic term of Morrow's elastoplastic strain-life curve usually leads to very conservative fatigue life or damage predictions.

Isotropic hardening and softening compete with mean stress relaxation mechanisms in strain-controlled cyclic deformations of structural alloys. To separate their effects, it is necessary to evaluate the relaxation of the mean stress, not of the maximum stress. Strain-controlled isotropic softening causes a gradual reduction of the maximum stress even in the absence of mean stress relaxation. Hence, the transient effects of mean stress relaxation and isotropic strain softening/hardening can be separated in uniaxial histories by studying, respectively, the evolution of the mean stress and the variation of the stress amplitude or range.

Mean stress relaxation is also found in multiaxial histories, caused by yield surface translations in unbalanced strain-controlled paths. It is present as well in multiaxial elastoplastic paths with mixed stress and strain control, as long as the relaxation direction is under strain control with an initial mean stress. For instance, exposed portions of buried pipelines may bear high static tensile and bending stresses in the axial direction due to ground or seabed displacements. Axial loadings in such long pipelines are usually assumed as strain controlled, therefore superimposed pressure cycles that cause plastic straining may result in a gradual relaxation of the axial stresses, increasing the fatigue life. Even though both hoop and radial histories are stress-controlled in the exposed pipeline portion due to the applied internal pressure, mean stress relaxation may happen in the strain-controlled axial direction of such partially-buried pipeline.

Mean stress relaxation can be quantitatively predicted from incremental plasticity simulations [15], if non-linear kinematic models are used to describe the associated asymmetrical behavior of the stress-strain curves, as studied in Part II of this work.

6. Conclusions

In this work, five-dimensional (5D) stress and strain spaces were proposed, representing a scaled version of Ilyushin's 5D spaces. These 5D spaces have several important properties, such as a metric proportional to Mises equivalent stresses or strains, the ability to represent yield surfaces using simple equations without scaling factors, and the possibility to work in reduced-order sub-spaces under free-surface conditions by simply removing appropriate rows from the stress and strain vectorial representations. The transformations to and from the proposed 5D spaces have been presented, providing an efficient framework to define incremental plasticity equations. These 5D spaces were applied to the qualitative study of uniaxial ratcheting, multiaxial ratcheting, and mean stress relaxation, through tension-torsion loading examples in 2D sub-spaces, and an unbalanced stress-controlled uniaxial loading example with significant mean stress. In Part II, a computationally-efficient incremental plasticity formulation is presented in the proposed 5D spaces, with the ability to model isotropic, non-proportional and non-linear kinematic hardening and thus to quantitatively predict ratcheting and mean stress relaxation effects, as verified from experimental measurements.

Acknowledgments

This work was supported in part by the National Natural Science Foundation of P.R. China under Grant #11302150. CNPq-Brazil provided fellowships for Profs. M.A. Meggiolaro and J.T.P. Castro.

References

[1] Kang, G. Ratcheting: Recent progresses in phenomenon observation, constitutive modeling and application. International Journal of Fatigue 2008;30:1448-1472.

[2] Ilyushin, AA. Plasticité, Éditions Eyrolles, Paris, 1956.

[3] Mandel, J. Cours de Mécanique des Milieux Continus, tomes I and II, Gauthier-Villars, Paris, 1966.

[4] Bishop, J.E. Characterizing the non-proportional and out-of-phase extend of tensor paths. Fatigue and Fracture of Engineering Materials and Structures 2000;23:1019-1032.

[5] Ilyushin, A.A. On the foundations of the general mathematical theory of plasticity. In: Voprosy Teorii Plastichnosti, Moskva: Izd. AN SSSR, 1961:3-29. (in Russian)

[6] Papadopoulos, I.V., Davoli, P., Gorla, C., Filippini, M., Bernasconi, A. A comparative study of multiaxial high-cycle fatigue criteria for metals. Int. Journal of Fatigue 1997;19:219-235.

[7] Tanaka, E. A nonproportionality parameter and a cyclic viscoplastic constitutive model taking into account amplitude dependences and memory effects of isotropic hardening. European Journal of Mechanics - A/Solids, 1994;13:155-173.

[8] Masing, G. Eigenspannungen and Verfestigung Beim Messing. Proceedings of the 2nd International Congress of Applied Mechanics, Zurich, Switzerland, 1926. (in German)

[9] Lim, C.-B., Kim, K.S., Seong, J.B. Ratcheting and fatigue behavior of a copper alloy under uniaxial cyclic loading with mean stress. International Journal of Fatigue 2009;31(3):501–507.

[10] Wang, Y., Yu, D., Chen, G., Chen, X. Effects of pre-strain on uniaxial ratcheting and fatigue failure of Z2CN18.10 austenitic stainless steel. International Journal of Fatigue 2013;52:106-113.

[11] Facheris, G., Janssens, K.G.F. Cyclic mechanical behavior of 316L: Uniaxial LCF and strain-controlled ratcheting tests. Nuclear Engineering and Design 2013;257:100-108.

[12] Chaboche, J.L. A review of some plasticity and viscoplasticity constitutive theories. International Journal of Plasticity 2008;24(10):1642-1693.

[13] Facheris, G., Janssens, K.G.F., Foletti, S. Multiaxial fatigue behavior of AISI 316L subjected to strain-controlled and ratcheting paths. International Journal of Fatigue 2014;68:195-208.

[14] Arcari, A., De Vita, R., Dowling, N.E. Mean stress relaxation during cyclic straining of high strength aluminum alloys. International Journal of Fatigue 2009;31(11-12):1742-1750.

[15] Landersheim, V., Bruder, T., Hanselka, H. Approximation of mean stress relaxation by numerical simulation using the Jiang model and extrapolation of results. Procedia Eng. 2011;10:595-600.

A general class of non-linear kinematic models to predict mean stress relaxation and multiaxial ratcheting in fatigue problems – Part II

Marco Antonio Meggiolaro[*,1], *Jaime Tupiassú Pinho de Castro*[1],
Hao Wu[2], *Eleazar Cristian Mejia Sanchez*[1]
[1]Department of Mechanical Engineering, Pontifical Catholic University of Rio de Janeiro, Brazil
[2]School of Aerospace Engineering and Applied Mechanics, Tongji University, Shanghai, P.R. China
meggi@puc-rio.br, jtcastro@puc-rio.br, wuhao@tongji.edu.cn, cris_ms10@hotmail.com

Abstract

Part I of this work introduced efficient reduced-order five-dimensional (5D) stress and strain spaces that can be used to predict ratcheting and mean stress relaxation phenomena at a much lower computation cost than in traditional 6D formulations. These 5D spaces were then applied to the qualitative study of uniaxial ratcheting, multiaxial ratcheting, and mean stress relaxation. Several non-linear kinematic (NLK) hardening models have been proposed to capture and quantify these effects in incremental plasticity simulations. In this Part II, an incremental plasticity formulation is proposed in the adopted 5D spaces, while its advantages over the classical 6D formulation are discussed. The 5D version of the main NLK models proposed in the literature are presented, which allows the definition of a unified generalized equation. The physical and geometrical interpretation of the hardening, dynamic recovery, and radial return terms from the proposed generalized equation are presented. Several surface translation rules can be represented as a particular case of the proposed model, including the ones by Chaboche (1983), Burlet-Cailletaud (1987), Ohno-Wang (1993), Jiang-Sehitoglu (1996), Bari-Hassan (2002) and Chen-Jiao (2005), among others. The adopted hardening surface representation can be used not only for the studied NLK models, but also to reproduce the Mróz-Garud multi-surface approach. Uniaxial ratcheting, multiaxial ratcheting, and mean stress relaxation experiments with 316L and 1020 steel tubular and cylindrical specimens are conducted to validate the proposed models.

Keywords: Multiaxial fatigue; Ratcheting; Incremental plasticity; Non-linear kinematic hardening; Non-proportional loading.

1. Introduction

The Bauschinger effect, observed under cyclic elastoplastic loading and also called *kinematic hardening*, is a change in the absolute value of the opposite yield strength after strain hardening, due to the microscopic stress distribution induced by the rearrangement of the dislocation structure inside the material associated with the plastic strains. Figure 1 exemplifies the Bauschinger effect for a uniaxial load history represented in the $\sigma_x \times \tau_{xy}\sqrt{3}$ von Mises diagram. In this example, the Mises yield surface $\sigma_{Mises} = S_Y$, which is the equation that describes the combinations of stress components that cause yielding, is allowed to translate with no change in its shape or radius $S = S_Y$. If the center of the yield surface is translated in the x direction of the Mises stress space by $(\sigma_{max} - S_Y)$, then the resulting surface will intersect the x axis in the new tensile yield stress $(\sigma_{max} - S_Y + S_Y) = \sigma_{max}$ and in the new compressive yield stress $(\sigma_{max} - S_Y - S_Y) = (\sigma_{max} - 2S_Y)$.

[*] Corresponding author. Tel.: +55-21-3527-1424; fax: +55-21-3527-1165. *E-mail:* meggi@puc-rio.br

The new center of the yield surface is commonly called *backstress*, represented here by the stress vector $\vec{\beta}$, which is responsible for storing such plastic memory efects. In this 2D example, the tensile yielding from the first cycle would change the backstress in the $\sigma_x \times \tau_{xy}\sqrt{3}$ diagram from its initial value $\vec{\beta} \equiv [\,\beta_x \;\; \beta_y\,]^T = [\,0 \;\; 0\,]^T$ to $\vec{\beta} \equiv [\,\beta_x \;\; \beta_y\,]^T = [\,\sigma_{max} - S_Y \;\; 0\,]^T$, see Fig. 1.

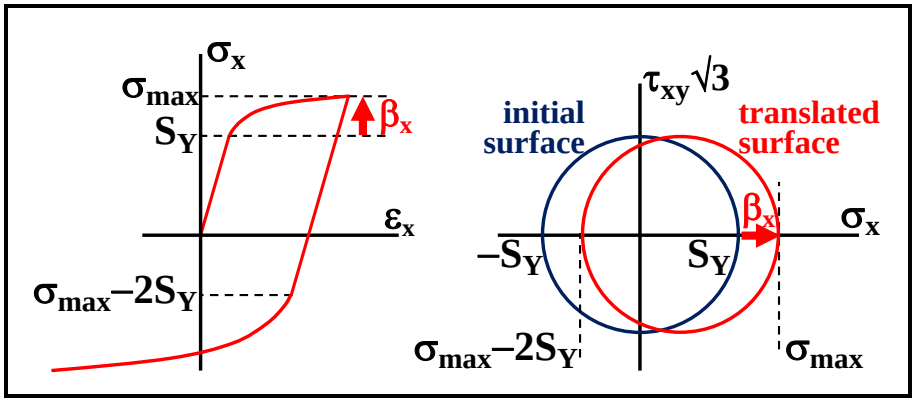

Fig. 1: Kinematic hardening in the *x* direction and associated Mises yield surface translation in the $\sigma_x \times \tau_{xy}\sqrt{3}$ diagram.

For a general multiaxial stress state, a 6D (instead of 2D) yield surface equation $Y = 0$ is adopted, usually based on the Mises criterion if the material is isotropic. So, the Mises yield surface can be represented as a hyper-sphere with radius $S \cdot \sqrt{2/3}$ in Voigt-Mandel's 6D deviatoric space, since

$$\vec{s} = \left[\, s_x \quad s_y \quad s_z \quad \tau_{xy}\sqrt{2} \quad \tau_{xz}\sqrt{2} \quad \tau_{yz}\sqrt{2} \,\right]^T \;\Rightarrow\; Y = (3/2)\cdot\left[\, |\vec{s}\,|^2 - (S\cdot\sqrt{2/3})^2 \,\right] = 0 \tag{1}$$

However, a much more convenient and computationally-efficient representation uses the E_{5s} stress space defined in Part I of this work, where the yield surface becomes a 5D hyper-sphere with radius *S*, since $|\vec{s}\,'| = S$, with the 5D deviatoric stress vector defined as

$$\vec{s}\,' \equiv \left[\, s_1 \quad s_2 \quad s_3 \quad s_4 \quad s_5 \,\right]^T = \left[\, \sigma_x - \frac{\sigma_y + \sigma_z}{2} \quad \frac{\sigma_y - \sigma_z}{2}\sqrt{3} \quad \tau_{xy}\sqrt{3} \quad \tau_{xz}\sqrt{3} \quad \tau_{yz}\sqrt{3} \,\right]^T \tag{2}$$

It was likewise shown in Part I that the 6D and 5D spaces are related by a 5×6 transformation matrix *A* through

$$\vec{s}\,' = A\cdot\vec{\sigma} = A\cdot\vec{s}, \quad \vec{e}\,'_{el} = A\cdot\vec{\varepsilon}_{el} = A\cdot\vec{e}_{el}, \quad \vec{e}\,'_{pl} = A\cdot\vec{\varepsilon}_{pl} = A\cdot\vec{e}_{pl} \tag{3}$$

where $\vec{\varepsilon}$, $\vec{e}$, and $\vec{e}\,'$ are respectively the 6D strain, 6D deviatoric strain, and 5D deviatoric strain, while the *el* and *pl* subscripts stand for their elastic and plastic components, and $\vec{\sigma}$ is the 6D stress. Note that the prime superscript refers to stresses and strains defined in the 5D space.

Hooke's law is essentially represented in the same way in both 6D and 5D deviatoric spaces, because the relations $\vec{s}\,' = A\cdot\vec{s}$ and $\vec{e}\,'_{el} = A\cdot\vec{e}_{el}$ imply that

$$\vec{e}_{el} = \vec{s}/2G \;\Rightarrow\; A\cdot\vec{e}_{el} = A\cdot\vec{s}/2G \;\Rightarrow\; \vec{e}\,'_{el} = \vec{s}\,'/2G \tag{4}$$

hence the deviatoric stress $\vec{s}\,'$ and elastic strain $\vec{e}\,'_{el}$ vectors are parallel and related by the scalar constant $2G$, a simple and convenient relation that further justifies the use of 5D stress and strain spaces.

Yet still not as popular as they should be, 5D formulations are not new. They have been originally proposed by Ilyushin [1], and have already been used in several multiaxial problems to calculate e.g.: (i) yield surface equations and failure criteria; (ii) path-equivalent stresses and strains using convex enclosures [2] or the Moment Of Inertia method [2-3]; (iii) multiaxial rainflow in the Modified Wang-Brown method [4]; and (iv) non-proportional hardening, using a 5D plastic strain space defined by Tanaka [5]. Nevertheless, incremental plasticity models are usually presented in a 6D formulation, performing 5D projections only after the calculation of the multiaxial stress-strain behavior, to perform multiaxial rainflow or path-equivalent calculations; or using a mixed 6D-5D formulation to compute non-proportional hardening transients, where 6D plastic strain increments are transformed to a 5D space at every cycle to compute Tanaka's 5×5 polarization matrix [5].

On the other hand, in this work the entire incremental plasticity formulation is presented in proper 5D spaces, through a formulation that is surprisingly almost identical to the 6D formulation, except for scaling factors such as the $\sqrt{2/3}$ from the yield surface equations. One of the main advantages of the proposed 5D spaces is that the entire incremental plasticity formulation can be easily reduced to 3D, 2D, or 1D only from the removal of appropriate rows from the deviatoric stress and strain vectors, as it was shown in Part I of this work. For instance, incremental plasticity calculations for a tension-torsion history could be performed in the 2D sub-spaces $\vec{s}_{2D} \equiv [s_1 \;\; s_3]^T$ and $\vec{e}_{2D} \equiv [e_1 \;\; e_3]^T$ defined in Part I. This dimensional reduction would decrease computational cost in more than 50%, especially if non-proportional hardening transients are modeled, adopting a 2×2 polarization matrix instead of Tanaka's original 5×5 version defined in [5].

Kinematic hardening e.g. can be modeled in the 5D formulation (or in its 3D, 2D, or 1D sub-spaces) by allowing the yield surface $|\vec{s}'|=S$ to translate its center from the origin of the E_{5s} space to a 5D backstress position $\vec{\beta}'$, becoming represented by $|\vec{s}'-\vec{\beta}'|=S$, with no change in its radius S or shape. Such translation is associated with plastic straining, usually assumed from the normality rule in the direction of the unit normal to the yield surface, defined as $\vec{n}$ for the 6D and $\vec{n}'$ for the adopted 5D formulation, evaluated at the current stress point. The Prandtl-Reuss plastic flow rule assumes that the magnitude of the plastic strain increment $d\vec{\varepsilon}_{pl}$ (in 6D) or $d\vec{\varepsilon}'_{pl}$ (in 5D) depends on the applied stress increment, being inversely proportional to the generalized plastic modulus P that defines the slope between stress and plastic strain increments. The Prandtl-Reuss rule is usually defined in tensor or 6D notation, but it is easy to show from the relations $\vec{n}' = A\cdot\vec{n}\cdot\sqrt{2/3}$, $\vec{n} = A^T\cdot\vec{n}'\cdot\sqrt{2/3}$, and $A\cdot A^T = 1.5\cdot I_{5\times5}$ (where $I_{5\times5}$ is the 5×5 identity matrix) that it has an almost identical version in the proposed 5D spaces, using the same P without even the need for a scaling factor:

$$d\vec{\varepsilon}_{pl} = (1/P)\cdot(d\vec{\sigma}^T\cdot\vec{n})\cdot\vec{n} = (1/P)\cdot(d\vec{s}^T\cdot\vec{n})\cdot\vec{n} \;\Rightarrow\; d\vec{\varepsilon}'_{pl} = (1/P)\cdot(d\vec{s}'^T\cdot\vec{n}')\cdot\vec{n}' \tag{5}$$

There are several models to calculate the current value of the generalized plastic modulus P as the yield surface translates, as well as the direction of such translation, to obtain the associated plastic strain increments. Most of these strain-hardening models can be divided into three classes: multi-surface [6-7], two-surface [8-9], and non-linear [10] kinematic hardening models.

Multi-surface kinematic hardening models assume that P is piecewise constant, resulting in a multi-linear description of the stress-strain curve, i.e. the non-linear shape of the stress-strain relation is approximated by several linear segments. Non-linear kinematic hardening models, on the other hand, are more general since they adopt non-linear equations to describe the surface translation direction and the value of P, leading to a more precise non-linear description of the stress-strain curve. A third class of kinematic hardening models involves the so-called two-surface models, which use a rather simplified formulation that combines elements of both non-linear and multi-surface kinematic models.

A major limitation of multi-surface models is that they cannot predict any uniaxial ratcheting or mean stress relaxation caused by unbalanced loadings, because their unrealistic perfectly symmetric hysteresis loops always close. In addition, under several non-proportional loading conditions, these models predict multiaxial ratcheting with a constant rate that never decays, severely overestimating the ratcheting effect measured in practice [11]. As a result, multi-surface kinematic hardening models should only be confidently applied to balanced proportional loading histories.

To correctly predict the stress-strain history associated with unbalanced loadings, it is necessary to use non-linear kinematic (NLK) hardening models. The original Armstrong and Frederick formulation [12] was improved by Chaboche [13], who indirectly introduced some multi-surface elements into the NLK models, however in a better non-linear instead of the simplistic multi-linear formulation.

In the following sections, the main NLK hardening models applicable to the prediction of ratcheting and mean stress relaxation are reviewed. A general hardening equation is presented, from which all NLK models are a special case. Moreover, this general equation is presented in the reduced-order five-dimensional space E_{5s} detailed in Part I of this work, which significantly decreases the computational cost in incremental plasticity calculations.

2. Multi-Surface and Non-Linear Kinematic (NLK) Hardening Models

Even though multi-surface models will not be simulated in this work, due to their inability to properly predict ratcheting and mean stress relaxation, their framework is detailed as follows. That is because Chaboche's 1979 contribution [13] to the original NLK models indirectly made them adopt essentially the same multi-surface formulation, as proven by Ohno and Wang in [14], however associated with non-linear instead of multi-linear incremental rules. The multi-surface formulation is presented next, in the proposed stress space E_{5s}.

2.1. Multi-surface formulation in 5D

Multi-surface models describe the strain-hardening behavior of elastoplastic solids from a family of nested yield surfaces in the stress space [6], the innermost being the yield surface associated with the initial yield strength S. In this work, instead of defining the nested surfaces in the 6D stress or 6D deviatoric stress spaces, the 5D reduced-order deviatoric stress space E_{5s} defined in Part I is adopted, using the Mises yield function to describe each surface. As mentioned before, this 5D space has several advantages over the 6D formulations, since it is a non-redundant representation of the deviatoric

stresses, which decreases the computational cost of stress-strain calculations. Although all kinematic hardening equations are presented here in the 5D space, their conversion to and from their original 6D versions is trivial, as it will be shown later.

Figure 2 shows the family of nested yield surfaces that store plastic memory, represented in a sub-space $s_1 \times s_2$ of the 5D space E_{5s}. The first and innermost circle in Fig. 2 is the initial yield surface (either monotonic or cyclic), with radius $r_1 \equiv S$ (without the need for the scaling factor $\sqrt{2/3}$). In addition, *$M-1$ hardening surfaces* with radii $r_1 < r_2 < \ldots < r_{M+1}$ are defined, along with an outermost *failure surface* whose radius r_{M+1} is equal to the true rupture stress σ_U of the material. Their centers are located at points $\vec{s}'_{ci}$ with $i = 2, 3, \ldots, M+1$, respectively. These $M+1$ nested circles cannot cross each other, must have increasing radii, and for a virgin material must be initially concentric at the origin of the E_{5s} space, i.e. initially their $\vec{s}'_{ci} = 0$. Moreover, the failure surface never translates, i.e. its center is always at the origin of the E_{5s} space, $\vec{s}'_{c_{M+1}} \equiv 0$. Indeed, any stress point that reaches its boundary causes the material to locally fracture due to ductility exhaustion, which is equivalent to the failure criterion $|\vec{s}'| = r_{M+1} = \sigma_U$.

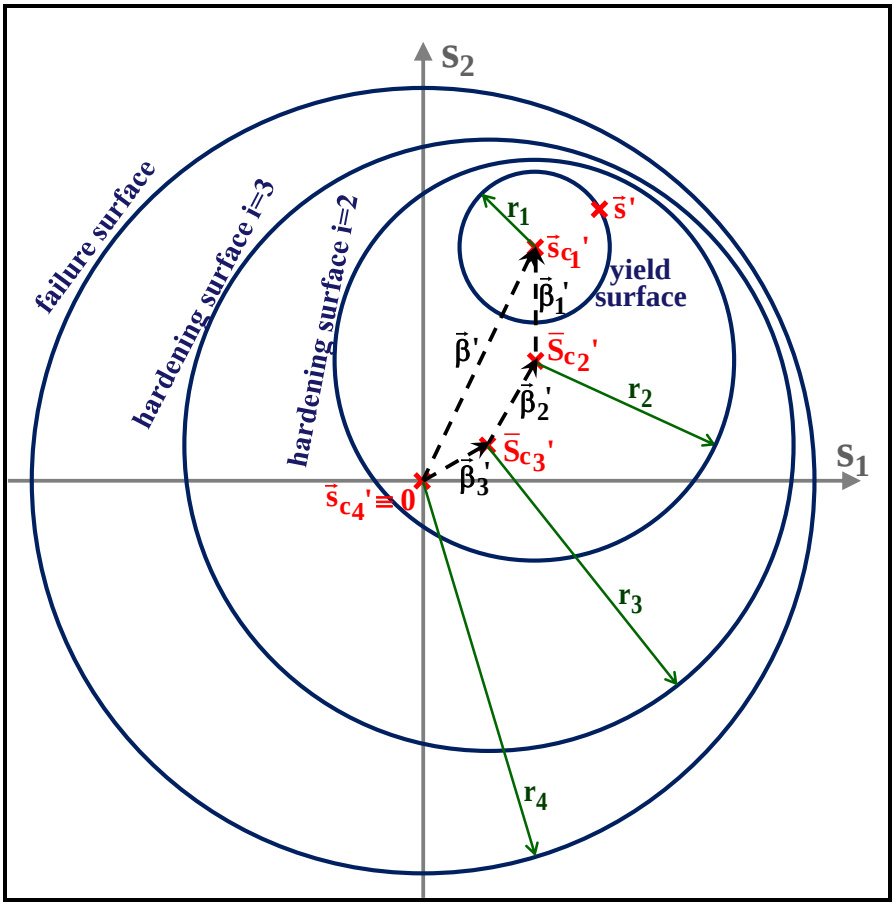

Fig. 2: Initial yield, hardening, and failure surfaces for $M = 3$ in the $s_1 \times s_2$ deviatoric stress sub-space of E_{5s}, showing the backstress vector $\vec{\beta}'$ that defines location of the yield surface center $\vec{s}'_{c1}$ and its components $\vec{\beta}'_1$, $\vec{\beta}'_2$, and $\vec{\beta}'_3$ that describe the relative positions between the centers of consecutive surfaces.

However, all other hardening surfaces can translate while the material strain-hardens, as shown in the arbitrary arrangement in Fig. 2. The surface centers move as the material plastically deforms and

hardens. The difference between the radii of each pair of consecutive surfaces in the proposed E_{5s} space is defined as $\Delta r_i \equiv r_{i+1} - r_i$. In principle, all radii r_i may change during plastic deformation as a result of isotropic and non-proportional hardening effects, whose description would require additional equations such as the Voce and Tanaka's rules [5].

The backstress vector $\vec{\beta}'$, which locates the current yield surface center $\vec{\beta}' \equiv \vec{s}'_{c1}$, can be decomposed as the sum of up to M surface backstresses $\vec{\beta}'_1$, $\vec{\beta}'_2$, …, $\vec{\beta}'_M$ that describe the relative positions $\vec{\beta}'_i = \vec{s}'_{ci} - \vec{s}'_{ci+1}$ between centers of consecutive yield surfaces, see Fig. 2 (which depicts a simple case with $M = 3$). Note that the length (norm) $|\vec{\beta}'_i|$ of each surface backstress in this 5D representation is always between $|\vec{\beta}'_i| = 0$, if the surface centers $\vec{s}'_{ci}$ and $\vec{s}'_{ci+1}$ coincide (as in the unhardened condition from Fig. 3), and $|\vec{\beta}'_i| = \Delta r_i$, if the surfaces are mutually tangent (a saturation condition with maximum hardening for the ith surface, see Fig. 3). In the saturated condition for surface i, the surface backstress $\vec{\beta}'_i$ is aligned with the normal vector $\vec{n}'$ that is perpendicular to these mutually tangent surfaces at the current deviatoric stress state $\vec{s}'$, see Fig. 3, resulting in $\vec{\beta}'_i = \vec{n}' \cdot (r_{i+1} - r_i) = \vec{n}' \cdot \Delta r_i$.

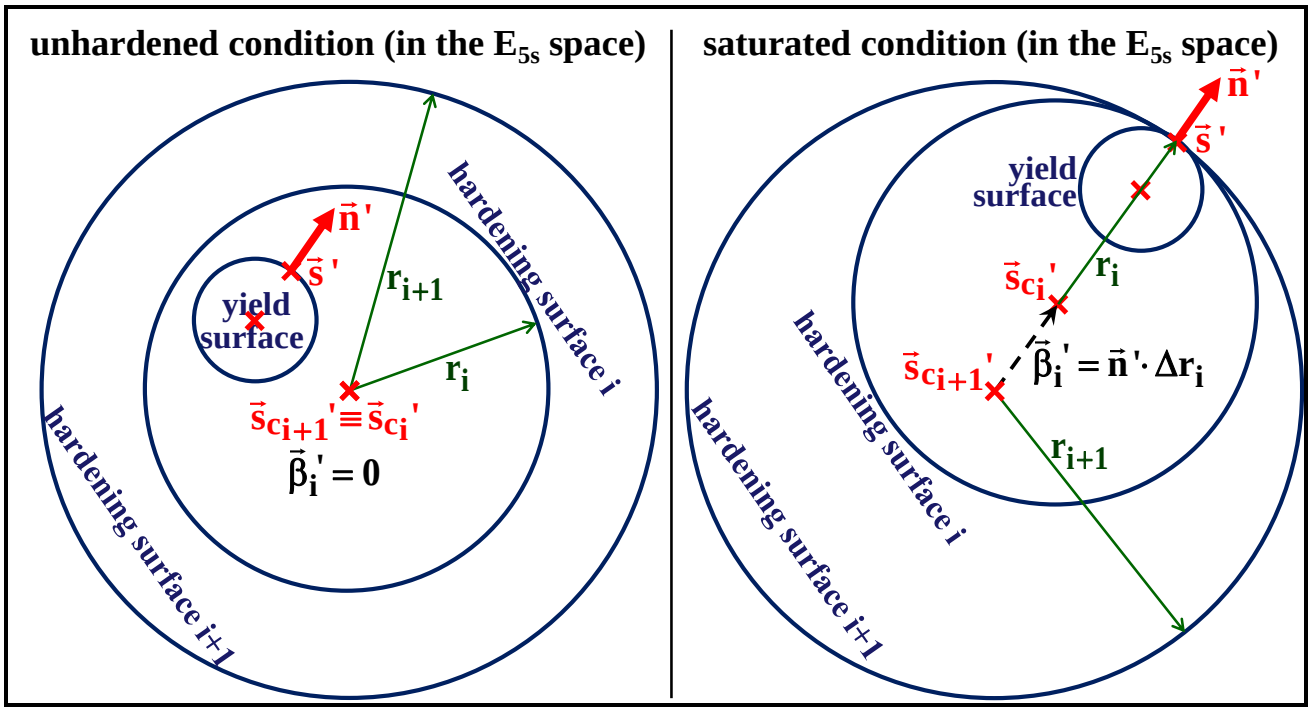

Fig. 3: Unhardened (left) and saturated (right) configurations of consecutive hardening surfaces i and $i+1$ in the proposed E_{5s} stress space, respectively associated with $\vec{\beta}'_i = 0$ and $\vec{\beta}'_i = \vec{n}' \cdot (r_{i+1} - r_i) = \vec{n}' \cdot \Delta r_i$.

2.2. Piecewise-constant multi-surface model drawbacks

The original multi-surface models proposed by Mróz [6] and Garud [7] use the above formulation (either in the original 6D version or in the proposed 5D spaces), however they assume that each hardening surface has its own generalized plastic modulus P, therefore it is piecewise-constant, generating a multi-linear description of the associated stress-strain curves. Such description usually provides good results for balanced proportional loadings, explaining their successful use in several multiaxial fatigue problems involving balanced loadings.

However, such multi-linear models cannot predict any uniaxial ratcheting or mean stress relaxation caused by unbalanced proportional loadings. This shortcoming is due to the linearity of the multi-surface translation rules and the resulting multi-linearity of the stress-strain representation, which describes all hysteresis loops using multiple straight segments, instead of predicting the experimentally observed curved paths caused by non-linear effects. Such straight segments generate unrealistic perfectly symmetric hysteresis loops that always close under constant amplitude proportional loadings, so this simplified formulation is unable to predict uniaxial ratcheting or mean stress relaxation.

In addition, for NP loadings, piecewise-constant multi-surface hardening models may predict multiaxial ratcheting with a constant rate that never decays, severely overestimating the ratcheting effect measured in practice. As a result, such multi-surface kinematic hardening models should only be applied to balanced loading histories, severely limiting their application.

These major drawbacks are a consequence of multi-surface kinematic hardening models being of an "uncoupled formulation" type, as qualified by Bari and Hassan in [15], meaning that the generalized plastic modulus P in the multi-surface formulation is not a function of the straining direction. Such "uncoupled procedure" provides undesirable additional degrees of freedom to the multi-surface models that allow, for instance, 90^o out-of-phase tension-torsion predictions with resulting plastic strain amplitudes that are not a monotonic function of the applied stress amplitudes, as they should be [16]. These wrong multi-surface predictions are both qualitatively and quantitatively dependent on the number of yield surfaces adopted in the model, without any clear convergence.

To correctly predict the stress-strain history associated with unbalanced loadings, it is necessary to couple the values of the generalized plastic modulus P and the straining direction, in addition to introducing non-linearity in the surface translation equations, generating the non-linear kinematic (NLK) models. Note that the same multi-surface formulation presented in Section 2.1 can be used for NLK models, using ideas presented in the seminal work by Chaboche [13], who indirectly introduced multi-surface elements into NLK models.

2.3. Multi-surface formulation in 5D for NLK hardening models

The first non-linear kinematic hardening model was proposed by Armstrong and Frederick in 1966 [12]. Their original single-surface model did not include any additional hardening surface, but their single yield surface already translated according to a non-linear rule. Since then, several improvements on Armstrong-Frederick's original NLK model have been proposed in the literature.

Fortunately, the exact same representation of the hardening behavior defined in Section 2.1 for the piecewise-constant multi-surface hardening models, which includes one inner initial yield surface, $M-1$ hardening surfaces, and one failure surface, can be used in the NLK hardening formulation, as it was demonstrated in [14]. Once again, instead of defining these yield surfaces in the 6D stress or deviatoric stress spaces, the proposed 5D reduced order deviatoric stress space E_{5s} is adopted, using the Mises yield function to describe each surface. Due to its many advantages, all kinematic hardening equations are presented in this 5D space, but their conversion to the 6D versions is trivial, as summarized in Table 1.

Table 1: Incremental plasticity equations using the proposed 5D or the classical 6D deviatoric formulations.

	proposed 5D Formulation	6D Formulation
Vector norm	$\lvert\vec{s}'\rvert = \sigma_{Mises}$	$\lvert\vec{s}\rvert = \sigma_{Mises}\sqrt{2/3}$
Hooke's law	$\vec{e}'_{el} = \vec{s}'/2G$, $d\vec{e}'_{el} = d\vec{s}'/2G$	$\vec{e}_{el} = \vec{s}/2G$, $d\vec{e}_{el} = d\vec{s}/2G$
Plastic flow rule	$d\vec{e}'_{pl} = (1/P)\cdot(d\vec{s}'^{T}\cdot\vec{n}')\cdot\vec{n}'$	$d\vec{\varepsilon}_{pl} = d\vec{e}_{pl} = (1/P)\cdot(d\vec{s}^{T}\cdot\vec{n})\cdot\vec{n}$
Direct problem	$d\vec{e}' = (d\vec{s}'/2G) + (1/P)\cdot(d\vec{s}'^{T}\cdot\vec{n}')\cdot\vec{n}'$ $d\vec{\varepsilon} = (2/3)\cdot A^{T}\cdot d\vec{e}' + d\vec{\sigma}_h/3\mathcal{K}$	$d\vec{e} = (d\vec{s}/2G) + (1/P)\cdot(d\vec{s}^{T}\cdot\vec{n})\cdot\vec{n}$ $d\vec{\varepsilon} = d\vec{e} + d\vec{\sigma}_h/3\mathcal{K}$
Inverse problem	$d\vec{s}' = 2G\cdot\left[d\vec{e}' - \frac{2G\cdot(d\vec{e}'^{T}\cdot\vec{n}')\cdot\vec{n}'}{2G+P}\right]$ $d\vec{\sigma} = 2A^{T}\cdot d\vec{s}'/3 + 3\mathcal{K}\cdot d\vec{\varepsilon}_h$	$d\vec{s} = 2G\cdot\left[d\vec{e} - \frac{2G\cdot(d\vec{e}^{T}\cdot\vec{n})\cdot\vec{n}}{2G+P}\right]$ $d\sigma = d\vec{s} + 3\mathcal{K}\cdot d\vec{\varepsilon}_h$
Normal vector	$\vec{n}' = \frac{\vec{s}'-\vec{\beta}'}{\sigma_{Mises}} = A\cdot n\cdot\sqrt{2/3}$	$\vec{n} = \frac{\vec{s}-\vec{\beta}}{\sigma_{Mises}\sqrt{2/3}} = A^{T}\cdot\vec{n}'\cdot\sqrt{2/3}$
Consistency	$d\vec{s}'^{T}\cdot\vec{n}' = d\vec{\beta}'^{T}\cdot\vec{n}' + dS$	$d\vec{s}^{T}\cdot\vec{n} = d\vec{\beta}^{T}\cdot\vec{n} + dS\cdot\sqrt{2/3}$
Surface radii	r_i (with $\Delta r_i = r_{i+1} - r_i$)	$r_i^* = r_i\sqrt{2/3}$ (with $\Delta r_i^* = \Delta r_i\sqrt{2/3}$)
NLK hardening	$d\vec{\beta}'_i = \begin{cases} p_i\cdot\vec{v}'_i\cdot d\mathcal{p}, & \text{if } \lvert\vec{\beta}'_i\rvert < \Delta r_i \\ 0, & \text{if } \lvert\vec{\beta}'_i\rvert = \Delta r_i \end{cases}$ $\vec{v}'_i = \vec{n}'\cdot\Delta r_i - \chi_i^*\cdot m_i^*\cdot\gamma_i\cdot$ $\cdot[\delta_i\cdot\vec{\beta}'_i + (1-\delta_i)\cdot(\vec{\beta}'^{T}_i\cdot\vec{n}')\cdot\vec{n}']$ $m_i^* \equiv \begin{cases} (\vec{\beta}'^{T}_i\cdot\vec{n}'/\lvert\vec{\beta}'_i\rvert)^{m_i}, & \text{if } \vec{\beta}'^{T}_i\cdot\vec{n}' \geq 0 \\ 0, & \text{if } \vec{\beta}'^{T}_i\cdot\vec{n}' < 0 \end{cases}$ $\chi_i^* \equiv (\lvert\vec{\beta}'_i\rvert/\Delta r_i)^{\chi_i}$ $P = \sum_{i=1}^{M}\frac{2p_i(\Delta r_i - \chi_i^*\cdot m_i^*\cdot\gamma_i\cdot\vec{\beta}'^{T}_i\cdot\vec{n}')}{3}$	$d\vec{\beta}_i = \begin{cases} p_i\cdot\vec{v}_i\cdot d\mathcal{p}, & \text{if } \lvert\vec{\beta}_i\rvert < \Delta r_i^* \\ 0, & \text{if } \lvert\vec{\beta}_i\rvert < \Delta r_i^* \end{cases}$ $\vec{v}_i = \vec{n}\cdot\Delta r_i^* - \chi_i^*\cdot m_i^*\cdot\gamma_i\cdot$ $\cdot[\delta_i\cdot\vec{\beta}_i + (1-\delta_i)\cdot(\vec{\beta}^{T}_i\cdot\vec{n})\cdot\vec{n}]$ $m_i^* \equiv \begin{cases} (\vec{\beta}^{T}_i\cdot\vec{n}/\lvert\vec{\beta}_i\rvert)^{m_i}, & \text{if } \vec{\beta}^{T}_i\cdot\vec{n} \geq 0 \\ 0, & \text{if } \vec{\beta}^{T}_i\cdot\vec{n} < 0 \end{cases}$ $\chi_i^* \equiv (\lvert\vec{\beta}_i\rvert/\Delta r_i^*)^{\chi_i}$ $P = \sqrt{\frac{2}{3}}\sum_{i=1}^{M} p_i(\Delta r_i^* - \chi_i^*\cdot m_i^*\cdot\gamma_i\cdot\vec{\beta}'^{T}_i\cdot\vec{n}')$

Similarly to the piecewise-constant multi-surface models, the backstress vector $\vec{\beta}'$ that locates the center of the current yield surface can be decomposed as the sum of *M* surface backstresses $\vec{\beta}'_1$, $\vec{\beta}'_2$, …, $\vec{\beta}'_M$ that describe the relative positions $\vec{\beta}'_i = \vec{s}'_{c_i} - \vec{s}'_{c_{i+1}}$ between the centers of consecutive yield surfaces, as proposed by Chaboche [13], significantly improving the Armstrong-Frederick model capabilities by indirectly introducing the concept of multiple hardening surfaces. Therefore, Figs. 2 and 3 and all their variables defined for the piecewise-constant multi-surface models can also be used in the NLK formulation.

One of their main differences is that in the piecewise-constant multi-surface models each hardening surface would only translate if the stress point was located on its border, while in NLK multi-

surface models all yield and hardening surfaces translate during a plastic straining process (but with different rates). The initial yield and the additional hardening surfaces from the NLK hardening models behave as if they were all attached to one another with non-linear spring-slider elements, causing coupled translations even before they enter in contact. Therefore, any yield surface translation causes all hardening surfaces to translate, usually with different magnitudes and directions, even before they become tangent to each other. Such coupling among surfaces allows the NLK models to introduce the necessary non-linearity in the stress-strain description.

Pairs of consecutive yield surfaces i and $i+1$ eventually become mutually tangent if $|\vec{\beta}_i'| = \Delta r_i$ (the 5D saturation condition), when their respective translations $d\vec{s}'_{c_i}$ and $d\vec{s}'_{c_{i+1}}$ will have the same magnitude and direction, therefore $d\vec{\beta}_i' = d\vec{s}'_{c_i} - d\vec{s}'_{c_{i+1}} = 0$, i.e. a zero surface backstress variation. In other words, in the proposed 5D formulation for the NLK hardening models, plastic straining causes increments $d\vec{\beta}_i' \neq 0$ in all backstress components, except for the saturated surfaces, therefore during plastic straining

$$d\vec{\beta}_i' = \begin{cases} p_i \cdot \vec{v}_i' \cdot dp, & if\ |\vec{\beta}'| < \Delta r_i \\ 0, & if\ |\vec{\beta}'| = \Delta r_i \end{cases}, \; i = 1, 2, \ldots, M \tag{6}$$

where $\vec{v}_i'$ is the translation direction vector for surface i, dp is the equivalent plastic strain increment, calculated in the proposed 5D E_{5p} plastic strain space as $dp = (2/3) \cdot |d\vec{e}'_{pl}|$, and p_i is a generalized plastic modulus coefficient that must be calibrated for every yield surface used in the calculation of of the generalized plastic modulus P.

The main difference among the several NLK hardening models proposed in the literature rests in the equation of the surface translation direction $\vec{v}_i'$. In the next section, a generalized surface translation rule is proposed in the adopted 5D E_{5s} stress space, which is able to unify all major NLK models into a single equation.

3. Generalized Surface Translation Rule

The generalized surface translation rule proposed in this work can be written as

$$\vec{v}_i' = \underbrace{\vec{n}' \cdot \Delta r_i}_{\substack{Prager- \\ Ziegler}} - \chi_i^* \cdot m_i^* \cdot \gamma_i \cdot [\ \underbrace{\delta_i \cdot \vec{\beta}_i'}_{\substack{dynamic \\ recovery}} + \underbrace{(1-\delta_i) \cdot (\vec{\beta}_i'^T \cdot \vec{n}') \cdot \vec{n}'}_{\substack{radial \\ return}}\ ] \tag{7}$$

where the scalar functions χ_i^* and m_i^* are defined as

$$\chi_i^* \equiv \left(\frac{|\vec{\beta}_i'|}{\Delta r_i} \right)^{\chi_i} \quad \text{and} \quad m_i^* \equiv \begin{cases} \left[\vec{\beta}_i'^T \cdot \vec{n}' / |\vec{\beta}_i'| \right]^{m_i}, & \text{if } \vec{\beta}_i'^T \cdot \vec{n}' \geq 0 \\ 0, & \text{if } \vec{\beta}_i'^T \cdot \vec{n}' < 0 \end{cases} \tag{8}$$

This function is a further generalization of the (already general) class of hardening rules defined by Jiang and Sehitoglu in [17], which only included the Prager-Ziegler and dynamic recovery terms from Eq. (7), but not the radial return term (discussed later on), i.e. it always assumed that $\delta_i = 1$.

The calibration parameters for each hardening surface i are the ratcheting exponent χ_i, the multiaxial ratcheting exponent m_i, the ratcheting coefficient γ_i, and the multiaxial ratcheting coefficient δ_i, which are scalar values listed in Table 2 for several popular models. Note that several references represent the NLK hardening parameters Δr_i, p_i and χ_i using respectively the terms $r^{(i)}$, $c^{(i)}$ and $\chi^{(i)}$, however this notation is not used in this work to avoid mistaking the (i) superscripts for exponents, as well as to emphasize the geometrical meaning of the Δr_i parameters, which are differences between radii of consecutive surfaces.

Table 2: Calibration parameters for the general translation direction from Eqs. (7-8).

Year	**Kinematic model**	$\boldsymbol{\chi_i}$	$\mathbf{m_i}$	$\boldsymbol{\gamma_i}$	$\boldsymbol{\delta_i}$
1949	Prager [18]	**0**	**0**	**0**	**1**
1966	Armstrong-Frederick [12]	**0**	**0**	$\mathbf{0 \le \gamma_i \le 1}$	**1**
1967	Mróz [6]	**0**	**0**	**1**	**1**
1979	Chaboche [13]	**1**	**0**	**1**	**1**
1986	Burlet-Cailletaud [20]	**0**	**0**	$\mathbf{0 \le \gamma_i \le 1}$	**0**
1993	Ohno-Wang I [21-22]	∞	**1**	**1**	**1**
1993	Ohno-Wang II [21-22]	$\mathbf{0 \le \chi_i} < \infty$	**1**	**1**	**1**
1995	Delobelle [24]	**0**	**0**	$\mathbf{0 \le \gamma_i \le 1}$	$\mathbf{0 \le \delta_i \le 1}$
1996	Jiang-Sehitoglu [17, 23]	$\mathbf{0 \le \chi_i} < \infty$	**0**	**1**	**1**
2004	Chen-Jiao [26]	$\mathbf{0 \le \chi_i} < \infty$	**1**	**1**	$\mathbf{0 \le \delta_i \le 1}$
2005	Chen-Jiao-Kim [25]	$\mathbf{0 \le \chi_i} < \infty$	$-\infty < \mathbf{m_i} < \infty$	**1**	**1**

The 5D translation direction $\vec{v}_i'$ of each yield surface from Eq. (7) can be separated into three components: (i) the Prager-Ziegler term, in the normal direction $\vec{n}'$ perpendicular to the yield surface; (ii) the dynamic recovery term, in the opposite direction $-\vec{\beta}_i'$ of the backstress induced by that yield surface, which acts as a recall term that gradually erases plastic memory with an intensity proportional to the product $\chi_i^* \cdot m_i^* \cdot \gamma_i \cdot \delta_i$; and (iii) the radial return term, in the opposite direction $-\vec{n}'$ of the normal vector, which affects multiaxial ratcheting predictions, calibrated from $\chi_i^* \cdot m_i^* \cdot \gamma_i \cdot (1-\delta_i) \cdot (\vec{\beta}_i'^T \cdot \vec{n}')$.

Figure 4 shows the geometric interpretation of these three components. The dynamic recovery term deviates the surface translation direction $\vec{v}_i'$ from the normal direction $\vec{n}'$, while the radial return term reduces the magnitude of the normal component from its original Prager-Ziegler term $\vec{n}' \cdot \Delta r_i$. Both dynamic recovery and radial return terms from each surface i are influenced by all four calibration parameters χ_i, m_i, γ_i and δ_i, which are further explained as follows.

Among the models included in Table 2, Prager's [18] translation direction $\vec{v}_i' = \vec{n}' \cdot \Delta r_i$ is not able to predict uniaxial ratcheting since it only uses the Prager-Ziegler term, which is linear. For multiaxial ratcheting, it only predicts a very short transient that almost immediately arrests reaching a shakedown state, highly underestimating multiaxial ratcheting rates. The translation direction $\vec{v}_i' = \vec{n}' \cdot \Delta r_i - \vec{\beta}_i'$

from Mróz [6] includes a dynamic recovery term, however in a linear formulation that highly overestimates multiaxial ratcheting effects. As discussed before, the Mróz rule cannot predict any uniaxial ratcheting at all when used in a multi-surface formulation, where the outer surfaces not touched by the current stress point are not allowed to translate. But when applied to the NLK formulation, where *all* surfaces translate during plastic straining, the Mróz translation direction becomes capable of predicting uniaxial ratcheting, albeit largely overestimating it.

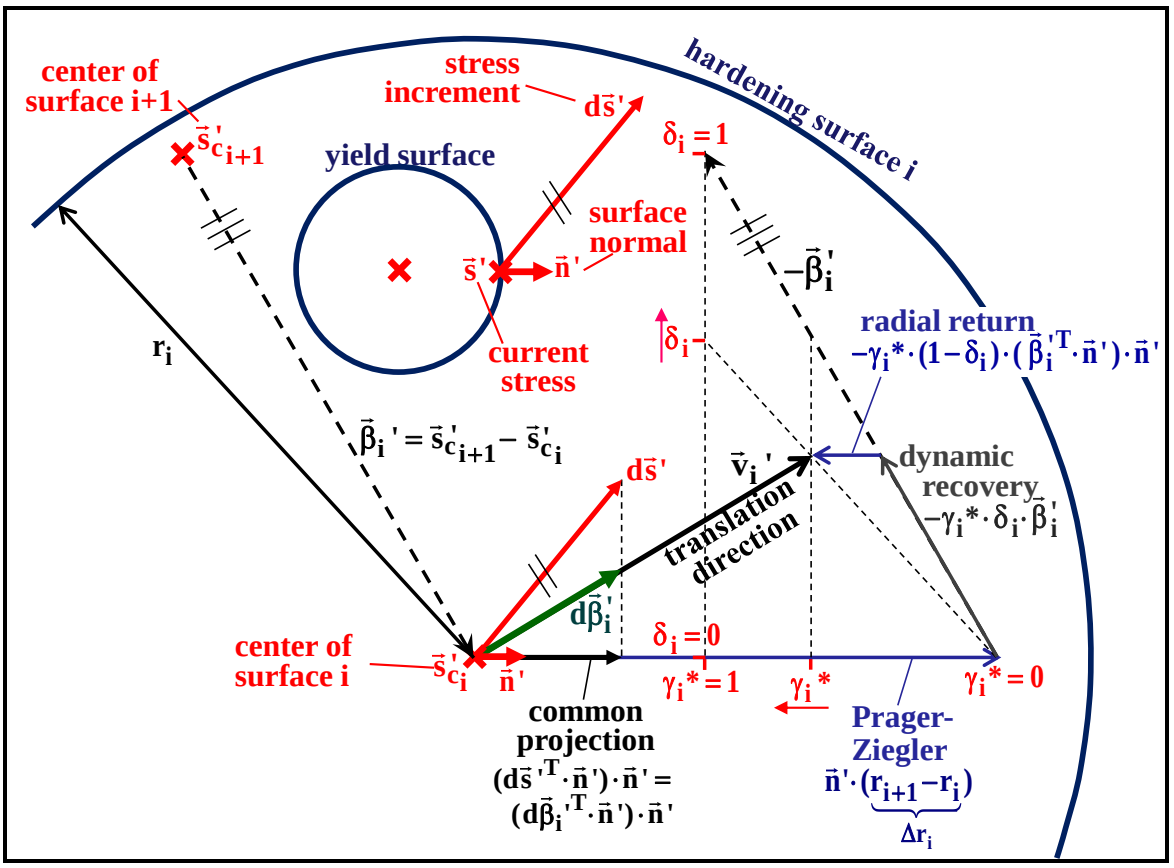

Fig. 4: Geometric interpretation of the three components of the translation direction $\vec{v}_i'$ of a hardening surface i, in the proposed E_{5s} stress space: Prager-Ziegler's, dynamic recovery, and radial return terms, where the equivalent parameter $\gamma_i^* \equiv \chi_i^* \cdot m_i^* \cdot \gamma_i$.

Armstrong and Frederick proposed the use of a ratcheting coefficient $0 \le \gamma_i \le 1$, originally intended to be a scalar function of the plastic strain path, adding non-linearity to their hardening model [12]. This parameter has been included in the proposed 5D general surface translation rule. However, in many practical implementations, γ_i was assumed as a constant, turning their translation equation $\vec{v}_i' = \vec{n}' \cdot \Delta r_i - \gamma_i \cdot \vec{\beta}_i'$ into a linear rule that suffers the same drawbacks of the Mróz translation rule in the NLK formulation, with a large overestimation of both uniaxial and multiaxial ratcheting. Even though γ_i can calibrate ratcheting rates, with the limit values $\gamma_i = 0$ (Prager's rule) for no ratcheting and $\gamma_i = 1$ (Mróz rule) for large ratcheting rates, the linearity associated with a constant γ_i makes it impossible to predict multiaxial ratcheting rate decay and arrest (shakedown) observed in several constant amplitude experiments. In addition, for constant coefficients $\gamma_i < 1$, the Armstrong-Frederick translation rule would result in $d\vec{\beta}_i' \neq 0$ in the saturated condition, which would allow the surfaces to

pass through one another. To avoid this, it has been proposed to simply enforce $\gamma_i = 1$ in the saturation condition $|\vec{\beta}_i'| = \Delta r_i$, while allowing the use of a calibrated $\gamma_i < 1$ for $|\vec{\beta}_i'| < \Delta r_i$ [19]. Both Armstrong-Frederick and Mróz rules are a particular case of the proposed generalized surface translation rule from Eqs. (7-8), for $\chi_i = m_i = 0$, $\delta_i = 1$, and an adjustable $0 \leq \gamma_i \leq 1$ that for Mróz is set to $\gamma_i = 1$.

Chaboche [13] replaced the constant ratcheting coefficient γ_i with a saturation ratio, which in the proposed 5D formulation is represented as $|\vec{\beta}_i'| / \Delta r_i$, ranging from 0 in the unhardened condition to 1 at saturation, eliminating the discontinuity problem caused by $\gamma_i \neq 1$. But even though the resulting surface translation rule (represented in its 5D version)

$$\vec{v}_i' = \vec{n}' \cdot \Delta r_i - (|\vec{\beta}_i'| / \Delta r_i) \cdot \vec{\beta}_i' \quad \text{(5D Chaboche)} \tag{9}$$

is an improvement over the constant γ_i models such as Mróz and most implementations of Armstrong-Frederick, it is unable to predict multiaxial ratcheting rate decay and arrest. This model predicts a short ratcheting transient followed by a constant ratcheting rate that never decays, overestimating its effects in multiaxial experiments. Chaboche's model is also a particular case of Eqs. (7-8), for $\chi_i = 1$, $m_i = 0$, and $\gamma_i = \delta_i = 1$.

Burlet and Cailletaud noticed that multiaxial experiments generally show lower ratcheting rates than the uniaxial ones for equivalent conditions on stress or strain amplitudes [20]. To lower the multiaxial ratcheting rate predictions without altering the uniaxial response, they replaced the dynamic recovery term with a radial return term. In the 5D formulation adopted in this work, their surface translation direction becomes

$$\vec{v}_i' = \vec{n}' \cdot \Delta r_i - \gamma_i \cdot (\vec{\beta}_i'^T \cdot \vec{n}') \cdot \vec{n}' \quad \text{(5D Burlet-Cailletaud)} \tag{10}$$

Burlet-Cailletaud's strain-hardening model is also obtained from the proposed Eqs. (7-8), assuming $\chi_i = m_i = \delta_i = 0$ and an adjustable $0 \leq \gamma_i \leq 1$.

The product $\vec{\beta}_i'^T \cdot \vec{n}'$ used in the radial return term measures the non-coaxiality between the surface backstress $\vec{\beta}_i'$ and the plastic strain increment direction $\vec{n}'$. As a result, it is a measure of the non-proportionality of the loading, since parallel $\vec{\beta}_i'$ and $\vec{n}'$ usually found in proportional loadings result in $\vec{\beta}_i'^T \cdot \vec{n}' = \pm |\vec{\beta}_i'|$, while 90^o out-of-phase loadings where plastic straining happens in a direction $\vec{n}'$ perpendicular to the surface backstress $\vec{\beta}_i'$ gives $\vec{\beta}_i'^T \cdot \vec{n}' = 0$. Such different products allow the model to predict non-proportional effects in multiaxial ratcheting.

In addition, the Burlet-Cailletaud's radial return term becomes identical to the Armstrong-Frederick's dynamic recovery term for uniaxial loadings, where parallel backstress $\vec{\beta}_i'$ and the normal to the yield surface $\vec{n}'$ vectors make $\gamma_i \cdot (\vec{\beta}_i'^T \cdot \vec{n}') \cdot \vec{n}' = \gamma_i \cdot \vec{\beta}_i'$; therefore, both models behave identically under uniaxial conditions, overpredicting uniaxial ratcheting rates. Note that Burlet-Cailletaud's yield surface translation direction $\vec{v}_i'$ is always parallel to $\vec{n}'$, therefore it behaves similarly to Prager's

rule under multiaxial loading conditions, largely underpredicting multiaxial ratcheting rates, which always rapidly decay in the simulations causing premature shakedown.

Ohno and Wang used the non-proportionality product (calculated in our 5D general formulation from $\vec{\beta}_i'^T \cdot \vec{n}'$) in a different way [21-22]. For plastic straining in a direction $\vec{n}'$ that makes an obtuse angle with $\vec{\beta}_i'$, i.e. when $\vec{\beta}_i'^T \cdot \vec{n}' < 0$ (usually during an elastoplastic unloading process), they assumed that the translation direction follows Prager's linear rule $\vec{v}_i' = \vec{n}' \cdot \Delta r_i$. Otherwise, when $\vec{\beta}_i'^T \cdot \vec{n}' \geq 0$ (usually during an elastoplastic loading process), they introduced in their model a scalar function (given by $0 \leq \chi_i^* \equiv (|\vec{\beta}_i'|/\Delta r_i)^{\chi_i} \leq 1$ in the proposed 5D formulation) and a non-proportionality term (defined in 5D as $0 \leq (\vec{\beta}_i'^T \cdot \vec{n}'/|\vec{\beta}_i'|) \leq 1$), resulting in the "Ohno-Wang II" (OW-II) surface translation direction, whose 5D version in the E_{5s} stress space becomes

$$\vec{v}_i' = \vec{n}' \cdot \Delta r_i - (|\vec{\beta}_i'|/\Delta r_i)^{\chi_i} \cdot (\vec{\beta}_i'^T \cdot \vec{n}'/|\vec{\beta}_i'|) \cdot \vec{\beta}_i' \quad \text{(5D Ohno-Wang II)} \tag{11}$$

where χ_i ($0 \leq \chi_i \leq \infty$) is the ratcheting exponent. Surfaces calibrated with a very large χ_i (such as in their "Ohno-Wang I" OW-I model version that assumes $\chi_i \to \infty$) have $\chi_i^* \cong 0$, which results in Prager's linear rule $\vec{v}_i' = \vec{n}' \cdot \Delta r_i$ for most of the range $0 \leq |\vec{\beta}_i'|/\Delta r_i \leq 1$ before saturation, becoming unable to predict uniaxial ratcheting. The dynamic recovery term would only be activated when the surfaces are closer to contacting each other, i.e. when $|\vec{\beta}_i'|/\Delta r_i \cong 1$. Lower calibrated values of χ_i, on the other hand, allow the dynamic recovery term to be partially operative in the entire $|\vec{\beta}_i'|/\Delta r_i$ range, increasing the predicted uniaxial ratcheting rates. So, in summary, lower calibrated values of χ_i result in higher uniaxial ratcheting rate predictions. Note that both OW-I and OW-II Ohno-Wang models are a particular case of the proposed Eqs. (7-8), adopting $m_i = \gamma_i = \delta_i = 1$, and an adjustable $0 \leq \chi_i < \infty$ that tends to infinity for the OW-I.

However, the ratcheting parameter χ_i influences both uniaxial and multiaxial ratcheting predictions. When χ_i is calibrated to fit uniaxial ratcheting data, the OW-II model ends up overestimating multiaxial ratcheting. In addition, although the OW-II model is able to predict multiaxial ratcheting rate decay, the use of a single calibration parameter χ_i renders it unable to model experiments with constant multiaxial ratcheting rates.

Jiang and Sehitoglu [17, 23] improved the OW-II model to solve this last problem by simply removing the non-proportionality term ($\vec{\beta}_i'^T \cdot \vec{n}'/|\vec{\beta}_i'|$ in our 5D formulation) from its translation rule. When represented in the proposed E_{5s} stress space, Jiang-Sehitoglu's surface translation direction is expressed as

$$\vec{v}_i' = \vec{n}' \cdot \Delta r_i - (|\vec{\beta}_i'|/\Delta r_i)^{\chi_i} \cdot \vec{\beta}_i' \quad \text{(5D Jiang-Sehitoglu)} \tag{12}$$

where $0 \leq \chi_i < \infty$. This equation is used even during an elastoplastic unloading $\vec{\beta}_i'^T \cdot \vec{n}' < 0$, instead of switching to Prager's linear rule as it had been proposed by Ohno and Wang.

Jiang-Sehitoglu's equation is also a particular case of Eqs. (7-8), for $m_i = 0$ and $\gamma_i = \delta_i = 1$, similar to Chaboche's model [13], and with an adjustable $0 \leq \chi_i < \infty$. As a result, Jiang-Sehitoglu's equation is a generalized version of Chaboche's original model [13], which would be obtained for the particular case $\chi_i = 1$. Since Chaboche's model has the ability to predict constant ratcheting rate for both uniaxial and multiaxial loadings, Jiang-Sehitoglu's equation overcomes the inability of the OW-II model to predict constant multiaxial ratcheting rates. Multiaxial ratcheting rate decay can also be predicted, if a ratcheting rate exponent $\chi_i \neq 1$ is chosen in the calibration. Nevertheless, Jiang-Sehitoglu's model still relies on a single calibration parameter χ_i to predict both uniaxial and multiaxial ratcheting rates.

Calibrating a kinematic hardening model using different parameters to independently control uniaxial and multiaxial ratcheting allows for a much better description of the material behavior. This separation is necessary because both ratcheting types are caused by different phenomena: uniaxial ratcheting is a consequence of anisotropy between the tension and compression behaviors, as discussed in Part I of this work, while multiaxial ratcheting is associated with elastoplastic deviatoric stress increments $d\vec{s}'$ that are not parallel to the normal $\vec{n}'$ to the yield surface at the current state, causing plastic strains not only in the direction of $d\vec{s}'$ but also ratcheting strains in perpendicular directions. For instance, a material with a significant strength difference between tension and compression could have almost the same multiaxial ratcheting behavior as a perfectly isotropic one, even though only the former could suffer uniaxial ratcheting. It would be impossible to accurately calibrate both independent behaviors with a single scalar parameter for each surface such as χ_i.

Since Armstrong-Frederick's model largely underpredicts while Burlet-Cailletaud's largely overestimates multiaxial ratcheting rates, Delobelle et al. [24] decided to interpolate them using a multiaxial ratcheting coefficient δ_i ($0 \leq \delta_i \leq 1$). In the proposed E_{5s} space, Delobelle's surface translation direction becomes

$$\vec{v}_i' = \vec{n}' \cdot \Delta r_i - \gamma_i \cdot [\delta_i \cdot \vec{\beta}_i' + (1-\delta_i) \cdot (\vec{\beta}_i'^T \cdot \vec{n}') \cdot \vec{n}'] \quad \text{(5D Delobelle)} \tag{13}$$

The limit value $\delta_i = 0$ gives exactly the Burlet-Cailletaud model, associated with a large radial return term and zero dynamic recovery, a "radial evanescence" condition that results in low multiaxial ratcheting rates with large rate decay. The other limit value $\delta_i = 1$ gives exactly the Armstrong-Frederick model, with a large dynamic recovery term and zero radial return, the usual "backstress evanescence" condition that results in overestimated multiaxial ratcheting without rate decay, as discussed before. If $0 < \delta_i < 1$, then the predictions are somewhere in between the two limit cases, with δ_i acting as a weighting factor to calibrate the multiaxial ratcheting rates. The value of γ_i influences both uniaxial and multiaxial ratcheting estimations. However, the uniaxial ratcheting response is not affected by δ_i because, for uniaxial loadings, $\vec{\beta}_i'$ and $\vec{n}'$ are always parallel to the uniaxial direction, therefore the relation $\gamma_i \cdot (\vec{\beta}_i'^T \cdot \vec{n}') \cdot \vec{n}' = \gamma_i \cdot \vec{\beta}_i'$ causes a translation direction

$$\vec{v}_i' = \vec{n}' \cdot \Delta r_i - \gamma_i \cdot [\delta_i + (1-\delta_i)] \cdot \vec{\beta}_i' = \vec{n}' \cdot \Delta r_i - \gamma_i \cdot \vec{\beta}_i' \quad \text{(5D Delobelle – uniaxial case)} \tag{14}$$

that is independent of δ_i. So, γ_i must be calibrated first for every surface to fit uniaxial ratcheting data, and after that the δ_i values can be freely calibrated to multiaxial ratcheting data without affecting the previous uniaxial calibration. Delobelle's model is obtained from the generalized surface translation rule from Eqs. (7-8) for $\chi_i = m_i = 0$, and adjustable $0 \le \gamma_i \le 1$ and $0 \le \delta_i \le 1$ to independently calibrate uniaxial and multiaxial ratcheting. Note however that, similarly to both Armstrong-Frederick and Burlet-Cailletaud equations, the Delobelle model still overpredicts uniaxial ratcheting rates, since the ratcheting coefficient γ_i is not as efficient as the ratcheting exponent χ_i to model uniaxial ratcheting rate decay or even growth as a function of the stress amplitude.

On the other hand, the Chen-Jiao-Kim model [25], in addition to the use of the better parameter χ_i to calibrate uniaxial ratcheting, is able to independently calibrate uniaxial and multiaxial ratcheting behaviors by incorporating a multiaxial ratcheting exponent m_i in the non-proportionality term $\vec{\beta}_i'^T \cdot \vec{n}' / |\vec{\beta}_i'|$ from the OW-II model. Therefore, for a multiaxial elastoplastic loading process with $\vec{\beta}_i'^T \cdot \vec{n}' \ge 0$, the scalar function $m_i^* \equiv (\vec{\beta}_i'^T \cdot \vec{n}' / |\vec{\beta}_i'|)^{m_i}$ is used to multiply the dynamic recovery term. In the proposed 5D formulation, Chen-Jiao-Kim's surface translation direction becomes

$$\vec{v}_i' = \vec{n}' \cdot \Delta r_i - (|\vec{\beta}_i'| / \Delta r_i)^{\chi_i} \cdot (\vec{\beta}_i'^T \cdot \vec{n}' / |\vec{\beta}_i'|)^{m_i} \cdot \vec{\beta}_i' \quad \text{(5D Chen-Jiao-Kim)} \tag{15}$$

where $0 \le \chi_i < \infty$ and $-\infty < m_i < \infty$. For an elastoplastic unloading process with $\vec{\beta}_i'^T \cdot \vec{n}' < 0$, Prager's linear rule $\vec{v}_i' = \vec{n}' \cdot \Delta r_i$ is used instead. For uniaxial load histories during elastoplastic loading, where the relation $\vec{\beta}_i'^T \cdot \vec{n}' = |\vec{\beta}_i'|$ is always valid, the scalar function m_i^* simply becomes $m_i^* = (1)^{m_i} = 1$, therefore uniaxial ratcheting predictions are not affected by the calibrated value of m_i. Thus, χ_i should be calibrated first for the yield and every hardening surface to fit uniaxial ratcheting rate data, and after that the m_i values could be freely calibrated to correctly describe measured multiaxial ratcheting rates and decays without affecting the previous uniaxial calibration. Chen-Jiao-Kim's model can also be obtained from the general Eqs. (7-8) proposed in this work, adopting $\gamma_i = \delta_i = 1$, and independently adjustable $0 \le \chi_i < \infty$ and $-\infty \le m_i \le \infty$.

A different approach for obtaining a simultaneous correct description of uniaxial and multiaxial ratcheting was adopted in the Chen-Jiao model [26]. This model uses Delobelle's [24] multiaxial ratcheting coefficient δ_i ($0 \le \delta_i \le 1$) instead of the multiaxial ratcheting exponent m_i, incorporated into Jiang-Sehitoglu's model to give, in the adopted E_{5s} space version,

$$\vec{v}_i' = \vec{n}' \cdot \Delta r_i - (|\vec{\beta}_i'| / \Delta r_i)^{\chi_i} \cdot [\delta_i \cdot \vec{\beta}_i' + (1 - \delta_i) \cdot (\vec{\beta}_i'^T \cdot \vec{n}') \cdot \vec{n}'] \quad \text{(5D Chen-Jiao)} \tag{16}$$

As in Delobelle's model, δ_i can calibrate multiaxial ratcheting data without affecting uniaxial ratcheting calculations. The exponent χ_i ($0 \le \chi_i < \infty$) of the yield or every hardening surface should be calibrated first to accurately match uniaxial ratcheting data, and only then the δ_i should be fitted to describe multiaxial ratcheting rates and decay. Chen and Jiao also refined the multiaxial ratcheting description, allowing the δ_i parameter from each surface to vary between an initial value and a target value δ_{ti}, with an evolution equation $d\delta_i = (\delta_{ti} - \delta_i) \cdot b_{CJ} \cdot dp$ controlled by the equivalent plastic

strain increments dp, where b_{CJ} is the Chen-Jiao evolution rate. Note however that this refinement introduces the additional parameters δ_{ti} (one for each surface i) and b_{CJ}, which would need to be calibrated in proper tests. Finally, note that Chen-Jiao's model is also a particular case of the proposed Eqs. (7-8), adopting $m_i = \gamma_i = 1$, and independently adjustable $0 \leq \chi_i < \infty$ and $0 \leq \delta_i \leq 1$.

Table 2 summarizes the calibration parameter choices for the general translation direction from Eqs. (7-8), showing that all presented models are a particular case of the proposed expression. Table 3 summarizes the advantages and disadvantages of the various equations that intend to describe the yield surface translation direction $\vec{v}_i'$. Note that independent calibration of uniaxial and multiaxial ratcheting rates can only be achieved using equations with at least two parameters per surface (i.e. a total of at least $2M$ parameters for M yield and hardening surfaces), such as the Delobelle, Chen-Jiao, and Chen-Jiao-Kim equations. However, Delobelle's model still overpredicts uniaxial ratcheting rates, due to the use of the ratcheting coefficient γ_i instead of the better ratcheting exponent χ_i to calibrate them. Nevertheless, if the studied load history only causes significant uniaxial or multiaxial ratcheting, but not both, then Jiang-Sehitoglu's equation would also be a good modeling choice, since it can calibrate arbitrary uniaxial or multiaxial ratcheting rates, including multiaxial ratcheting with constant rate or rate decay, using only the M ratcheting exponents χ_i from the M surfaces, without requiring the (possibly less robust) calibration of $2M$ or more parameters.

Table 3: Characteristics of the various NLK surface translation direction models regarding number of parameters to be calibrated (NPC) for M surfaces (assuming that the Δr_i and p_i from each yield surface have been identified) and ability to accurately model all uniaxial ratcheting conditions including rate decay (UR), or all multiaxial ratcheting conditions with constant rate (MRC) or with rate decay (MRD), to calibrate arbitrary uniaxial (U) or multiaxial ratcheting rates (M), and to independently calibrate arbitrary uniaxial and multiaxial ratcheting rates (UM).

Year	Kinematic model	NPC	UR	MRC	MRD	U	M	UM
1949	Prager [18]	**0**						
1966	Armstrong-Frederick [12]	**M**		✓		✓	✓	
1967	Mróz [6]	**0**		✓				
1979	Chaboche [13]	**0**		✓				
1986	Burlet-Cailletaud [20]	**M**			✓	✓	✓	
1993	Ohno-Wang I [21-22]	**0**			✓			
1993	Ohno-Wang II [21-22]	**M**	✓		✓	✓	✓	
1995	Delobelle [24]	**2M**		✓	✓	✓	✓	✓
1996	Jiang-Sehitoglu [17, 23]	**M**	✓	✓	✓	✓	✓	
2004	Chen-Jiao [26]	**2M**	✓	✓	✓	✓	✓	✓
2004	Chen-Jiao (refined) [26]	**3M+1**	✓	✓	✓	✓	✓	✓
2005	Chen-Jiao-Kim [25]	**2M**	✓	✓	✓	✓	✓	✓

The fitting of the generalized plastic modulus coefficients p_i from each surface for a given Δr_i, see Eq. (6), as well as the calibration of the ratcheting coefficients χ_i, m_i, γ_i, and/or δ_i, depend on the adopted NLK model. Approximate fitting algorithms for the parameter pairs (p_i, χ_i) or (Δr_i, χ_i) are shown in [23] for Jiang-Sehitoglu's model, which can be easily adapted from the 6D to the proposed

5D formulation, however they are precise only for materials with very large ratcheting exponents χ_i. For other cases, a least-squares fitting approach should be adopted to calibrate such parameters, comparing experimental measurements with incremental plasticity simulations.

4. Consistency Condition Formulation in 5D

Any straining process within the yield surface is assumed purely elastic, so from Hooke's law in Eq. (4) the stress and elastic strain increments in 5D are related by $d\vec{e}'_{el} = d\vec{s}'/2G$. A plastic straining process beyond the yield surface would make it translate according to Eq. (6), preventing the stress state from crossing outside its boundary. The mathematical condition that guarantees that the new stress state $\vec{s}' + d\vec{s}'$ during a plastic process will remain on the yield surface border, without crossing outside it, is called consistency condition. Such infinitesimal condition can be calculated in the proposed E_{5s} space forcing the yield surface equation $Y = (\vec{s}' - \vec{\beta}')^T \cdot (\vec{s}' - \vec{\beta}') - S^2 = 0$ to remain valid throughout the surface translation process, thus

$$dY = 2 \cdot d\vec{s}'^T \cdot (\vec{s}' - \vec{\beta}') - 2 \cdot d\vec{\beta}'^T \cdot (\vec{s}' - \vec{\beta}') - 2 \cdot S \cdot dS = 0 \tag{17}$$

and, since the normal unit vector is such that $\vec{n}' = (\vec{s}' - \vec{\beta}')/|\vec{s}' - \vec{\beta}'| = (\vec{s}' - \vec{\beta}')/S$, then

$$d\vec{s}'^T \cdot \vec{n}' = d\vec{\beta}'^T \cdot \vec{n}' + dS \quad \text{(5D consistency condition)} \tag{18}$$

The scalar dS term in the consistency condition accounts for the variation of the yield surface radius S, gradually changing from the monotonic $S = S_Y$ to the cyclic $S = S_{Yc}$ in isotropic hardening and, in non-proportional (NP) loadings, to an NP-hardened yield strength $S = S_{YNP}$.

In the proposed incremental plasticity formulation, without loss of generality, instead of varying the radii $r_1 = S$ of the yield and r_i of the hardening surfaces (and consequently the radius differences $\Delta r_i \equiv r_{i+1} - r_i$), they are assumed constant, while isotropic and NP hardening effects are accounted for by changing the generalized plastic modulus coefficients p_i (instead of the Δr_i). Therefore, in this formulation where the yield surface radius $r_1 = S$ is assumed constant and thus $dS = 0$, the 5D consistency condition from Eq. (18) simplifies to $d\vec{s}'^T \cdot \vec{n}' = d\vec{\beta}'^T \cdot \vec{n}'$. Since the backstress increment $d\vec{\beta}'$ consists of the sum of the various backstress component increments $d\vec{\beta}' = d\vec{\beta}'_1 + d\vec{\beta}'_2 + ... + d\vec{\beta}'_M$, where each one has been defined in Eq. (6) as $d\vec{\beta}'_i = p_i \cdot \vec{v}'_i \cdot dp$, it follows that the consistency condition $d\vec{s}'^T \cdot \vec{n}' = d\vec{\beta}'^T \cdot \vec{n}'$ gives

$$d\vec{s}'^T \cdot \vec{n}' = d\vec{\beta}'^T \cdot \vec{n}' = (p_1 \cdot \vec{v}_1'^T \cdot \vec{n}' + p_2 \cdot \vec{v}_2'^T \cdot \vec{n}' + ... + p_M \cdot \vec{v}_M'^T \cdot \vec{n}') \cdot dp \tag{19}$$

In this formulation with the various yield surface radii r_i assumed constant, the values of p_i are initially calibrated to each surface using e.g. the monotonic stress-strain curve, and then corrected at every load cycle assuming they are directly proportional to the isotropic or NP hardening factors. For instance, after uniaxial isotropic hardening stabilization, every p_i would be multiplied by the S_{Yc}/S_Y ratio between the cyclic and monotonic yield strengths. In this way, it would be possible to assume constant yield and hardening surface radii without altering the stress-strain predictions.

The plastic flow rule in the proposed 5D deviatoric representation gives

$$d\vec{e}'_{pl} = \frac{1}{P}\cdot(d\vec{s}'^{T}\cdot\vec{n}')\cdot\vec{n}' \Rightarrow d\vec{s}'^{T}\cdot\vec{n}' = P\cdot\underbrace{d\vec{e}'^{T}_{pl}\cdot\vec{n}'}_{(3/2)\cdot dp} \Rightarrow P = \frac{2}{3}\cdot\frac{d\vec{s}'^{T}\cdot\vec{n}'}{dp} \tag{20}$$

Therefore, the generalized plastic modulus P needed to compute plastic straining can be expressed as a function of $\vec{v}'_i$ (as it would be expected for any "coupled formulation" [15]) through

$$P = (2/3)\cdot(p_1\cdot\vec{v}'^{T}_1 + p_2\cdot\vec{v}'^{T}_2 + ... + p_M\cdot\vec{v}'^{T}_M)\cdot\vec{n}' \tag{21}$$

The projections $\vec{v}'^{T}_i\cdot\vec{n}'$ of the generalized surface translation directions from Eq. (7) are given by

$$\vec{v}'^{T}_i\cdot\vec{n}' = \Delta r_i - \chi_i^*\cdot m_i^*\cdot\gamma_i\cdot[\delta_i + (1-\delta_i)]\cdot\vec{\beta}'^{T}_i\cdot\vec{n}' = \Delta r_i - \chi_i^*\cdot m_i^*\cdot\gamma_i\cdot\vec{\beta}'^{T}_i\cdot\vec{n}' \tag{22}$$

which, when combined to Eq. (21), allow the calculation of the associated generalized plastic modulus

$$P = (2/3)\cdot\sum_{i=1}^{M} p_i\cdot(\Delta r_i - \chi_i^*\cdot m_i^*\cdot\gamma_i\cdot\vec{\beta}'^{T}_i\cdot\vec{n}') \tag{23}$$

For a given 5D stress increment $d\vec{s}' = A\cdot d\vec{\sigma}$, such P could then be used in the 5D version of the Prandtl-Reuss flow rule in Eq. (5) to obtain the total strain increment

$$d\vec{e}' = d\vec{e}_{el} + d\vec{e}'_{pl} = \frac{d\vec{s}'}{2G} + \frac{1}{P}(d\vec{s}'^{T}\cdot\vec{n}')\cdot\vec{n}' \tag{24}$$

On the other hand, for a given 5D total strain increment $d\vec{e}' = A\cdot d\vec{\varepsilon}$, the 5D inverse problem could be solved (after some algebraic manipulation) by

$$d\vec{s}' = 2G\cdot d\vec{e}' - 2G\cdot\left[\frac{2G}{2G+P}d\vec{e}'^{T}\cdot\vec{n}'\right]\cdot\vec{n}' \tag{25}$$

After the entire stress or strain incremental integration in the computationally-efficient 5D spaces, the corresponding 6D values could be retrieved from the transformations described in Part I of this work:

$$\begin{cases}\vec{\sigma} = (2/3)A^{T}\cdot\vec{s}' + \vec{\sigma}_h \\ \vec{\varepsilon} = (2/3)A^{T}\cdot\vec{e}' + \vec{\varepsilon}_h\end{cases} \tag{26}$$

where the linear elastic hydrostatic components (assuming pressure-insensitive materials such as most metals) are easily calculated from the elastic relation $\vec{\sigma}_h = 3K\cdot\vec{\varepsilon}_h$, where $K = E/[3\cdot(1-2\nu)]$ is the bulk modulus of the material.

5. Isotropic and NP Hardening Formulation in 5D

Isotropic and non-proportional (NP) hardening transients could also be incorporated into the proposed 5D NPH formulation, through the varying values of the generalized plastic modulus coefficients p_i from each yield and hardening surface. From the Voce isotropic law and Tanaka's NP hardening equations [5], the values of p_i could be calculated as a function of the accumulated plastic strain $p \equiv \int dp$ from

$$p_i(p) = \underbrace{p_{ci} \cdot [1 + \alpha_{NP} \cdot F_{NP}(p)]}_{NP\ evolution} + \underbrace{(p_{mi} - p_{ci}) \cdot e^{-hr_c \cdot p}}_{isotropic\ evolution} \tag{27}$$

where p_{mi} and p_{ci} are the p_i coefficients calibrated respectively under uniaxial monotonic and cyclic conditions, hr_c is the material-dependent isotropic hardening rate, α_{NP} is the material-dependent additional hardening coefficient caused by non-proportional loads (with $0 \leq \alpha_{NP} \leq 1$), and $F_{NP}(p)$ is the load-path-dependent non-proportionality factor (with $0 \leq F_{NP}(p) \leq 1$).

The $F_{NP}(p)$ values are obtained in Tanaka's model [5] from a 5×5 polarization tensor $[P_T]$, whose evolution is given by

$$[dP_T] = (\vec{n}' \cdot \vec{n}'^T - [P_T]) \cdot hr_T \cdot dp \tag{28}$$

where hr_T is the material-dependent polarization rate and $\vec{n}'$ is the unit plastic straining direction in the proposed E_{5p} plastic strain space. From Tanaka's original model, it can be shown that the evolution equation of $F_{NP}(p)$ is given by

$$dF_{NP}(p) = \left[\sqrt{2 - \frac{2 \cdot \left| [P_T] \cdot \vec{n}' \right|^2}{tr\left([P_T]^T \cdot [P_T] \right)}} - F_{NP}(p) \right] \cdot hr_{NP} \cdot dp \tag{29}$$

where $tr(.)$ is the trace function, and hr_{NP} is the material-dependent NP hardening rate. Note that histories under free-surface conditions could adopt 3D or 2D sub-spaces of the defined 5D spaces, where Tanaka's tensor would be represented respectively as 3×3 or 2×2 matrices, greatly reducing computational cost while evaluating Eq. (28) at every cycle. This is another major advantage of the 5D incremental plasticity formulation proposed in this work.

6. Notch Formulation in 5D

The presented 5D spaces could also consider notch effects, without having to deal with 6D or tensor formulations. Two major 5D approaches for accounting for stress/strain concentration effects at notch tips could be followed: Pseudo-Material and Incremental Neuber or Molski-Glinka. Their application to the 5D formulation is discussed next.

6.1. Pseudo-material approach in 5D

For a given nominal stress history, the Pseudo-Material approach [27] could be used in 5D through the calibration of the generalized plastic modulus coefficients p_i to a fictitious material (a pseudo-material) with stress-strain behavior given by a nominal stress × notch strain curve, calculated under uniaxial conditions from a strain concentration rule such as Neuber or Molski-Glinka [28]. The 5D incremental plasticity formulation calibrated to this pseudo-material would then be used to calculate the notch-root strain history from the given multiaxial nominal stresses. After the entire notch strain history is obtained, the 5D incremental plasticity formulation is applied once more, but calibrated to the actual material properties (not the pseudo-material properties) to find the multiaxial notch stresses from the previously calculated multiaxial notch strains.

Conversely, for a given nominal strain history, a pseudo-material would be calibrated with stress-strain behavior given by a notch stress × nominal strain curve, calculated from a uniaxial model such as Neuber or Molski-Glinka. The notch-root stresses would then be calculated in the 5D formulation from the given nominal strains using the pseudo-material properties. The notch stress history is then input to a 5D incremental algorithm calibrated to the actual material properties, to find the corresponding multiaxial notch strains.

6.2. Incremental Neuber or Molski-Glinka

The original Neuber rule was derived for prismatic bodies loaded in pure shear, stating an equivalence between distortional strain energy densities, without including dilatational energies (which are zero under pure shear). Since Neuber's original relation did not include the dilatational strain energy density, Neuber's rule should assume that the total *distortional* strain energy density is constant for the pseudo and notch stress-strain curves [29]. Therefore, Neuber's incremental rule [30] adopts an equivalence of deviatoric stress and strain products, eliminating the influence of the hydrostatic components. Using the 6D-to-5D transformations defined in Part I of this work, it can be shown that Neuber's incremental rule can be represented in the proposed 5D formulation simply from

$$s_i \cdot de_i + e_i \cdot ds_i = \tilde{s}_i \cdot d\tilde{e}_i + \tilde{e}_i \cdot d\tilde{s}_i \quad \text{(5D Incremental Neuber)} \tag{30}$$

for $i = 1, 2, \ldots, 5$, where $\tilde{s}_i$ and $\tilde{e}_i$ are pseudo-values calculated (e.g. in a Finite Element program) assuming linear-elastic conditions, and s_i and e_i are the associated elastoplastic notch-tip values. Molski-Glinka's rule [28] could also be used in an incremental deviatoric way in the proposed 5D formulation resulting, for $i = 1, 2, \ldots, 5$, in

$$s_i \cdot de_i = \tilde{s}_i \cdot d\tilde{e}_i \quad \text{(5D Incremental Molski-Glinka)} \tag{31}$$

One inconvenience of this approach (either in the original 6D or in the proposed 5D versions) is that it requires the solution of a set of equations such as the ones from Eq. (30) or (31), which can be computationally costly in an implicit integration formulation.

Finally, a Modified Boundary Condition approach [31] could also be followed, easily adaptable to the proposed 5D formulation since a single strain energy equation is required, with the remaining equations coming from assumptions on the ratios of pseudo and notch components. Such problems are most important for practical applications, and they will be further explored in future works.

7. Experimental Validation

The proposed 5D incremental plasticity formulation has been implemented in the ViDa 3D software [32] to predict multiaxial elastoplastic stress-strain relations. Isotropic, non-proportional (NP), and all presented non-linear kinematic hardening models were simulated in the 5D formulation for various representative loading paths. The numerical robustness of the algorithm was verified using the same model in both stress and strain control, as recommended in [33], i.e. the stress history is calculated in the code from a given strain history, and then the computed stresses are used as input to the same code to predict the original strain history, with negligible errors of the order of the computation resolu-

tion. A large number of conducted simulations using unbalanced load histories confirmed all conclusions summarized in Table 3 about the characteristics of different kinematic hardening models. Like the notch problems, such simulations will be further explored elsewhere. However, a few experimental problems are discussed following to illustrate the power of the proposed methodology.

For the experimental verification, simulations were performed using the proposed generalized surface translation rule from Eqs. (7-8), calibrated to describe Jiang-Sehitoglu's model. To improve the calculation accuracy, the backstress was divided into 10 additive components, following Chaboche's idea [13], with stress increments at each integration step limited to only 2MPa. Jiang-Sehitoglu's material parameters were calibrated from uniaxial data using the procedure described in [23].

Tension-torsion experiments were performed on tubular annealed 316L stainless steel specimens in an MTS multiaxial testing machine, see Fig. 5. The cyclic properties of this steel were obtained from uniaxial tests. Engineering stresses and strains were measured using a load/torque cell and an MTS axial/torsional extensometer.

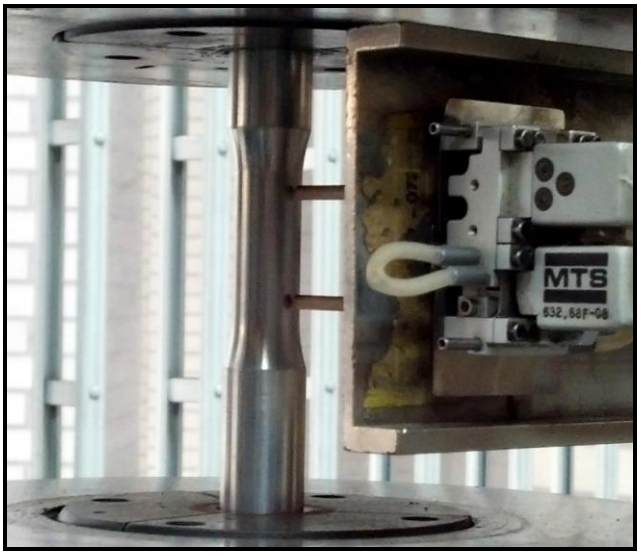

Fig. 5: Tubular specimen mounted in an MTS tension-torsion machine, showing the axial/torsional extensometer.

One of the experimented strain-controlled tension-torsion tests adopted strain paths describing a square pulse in the $\varepsilon_x \times \gamma_{xy}/\sqrt{3}$ strain diagram, see Fig. 6. The predicted and measured stress paths after isotropic and NP hardening stabilization show good agreement even in the presence of significant mean stress relaxation, as it can be observed from the low resulting mean stresses in the almost symmetrical stress paths, despite the high applied mean strains. The same calibrated parameters from the proposed generalized surface translation rule were later used to predict multiaxial ratcheting under stress control, also showing a very good experimental agreement. These results confirm that ratcheting and mean stress relaxation are indeed two aspects of the same phenomenon, which become evident respectively under stress and strain control.

To evaluate the ability of the proposed formulation to predict as well uniaxial ratcheting, uniaxial tension-compression experiments were performed on cylindrical specimens made of 1020 steel with

yield strength 365MPa and ultimate strength 542MPa. An unbalanced history between *–200* and *350MPa* was imposed under stress control, with a mean stress component that induced uniaxial ratcheting, see Fig. 7. As shown in the figure, by adopting a calibration that describes Jiang-Sehitoglu's kinematic hardening model, the proposed formulation is able to predict reasonably well the ratcheting rate decay observed in the first 100 cycles of such unbalanced loading.

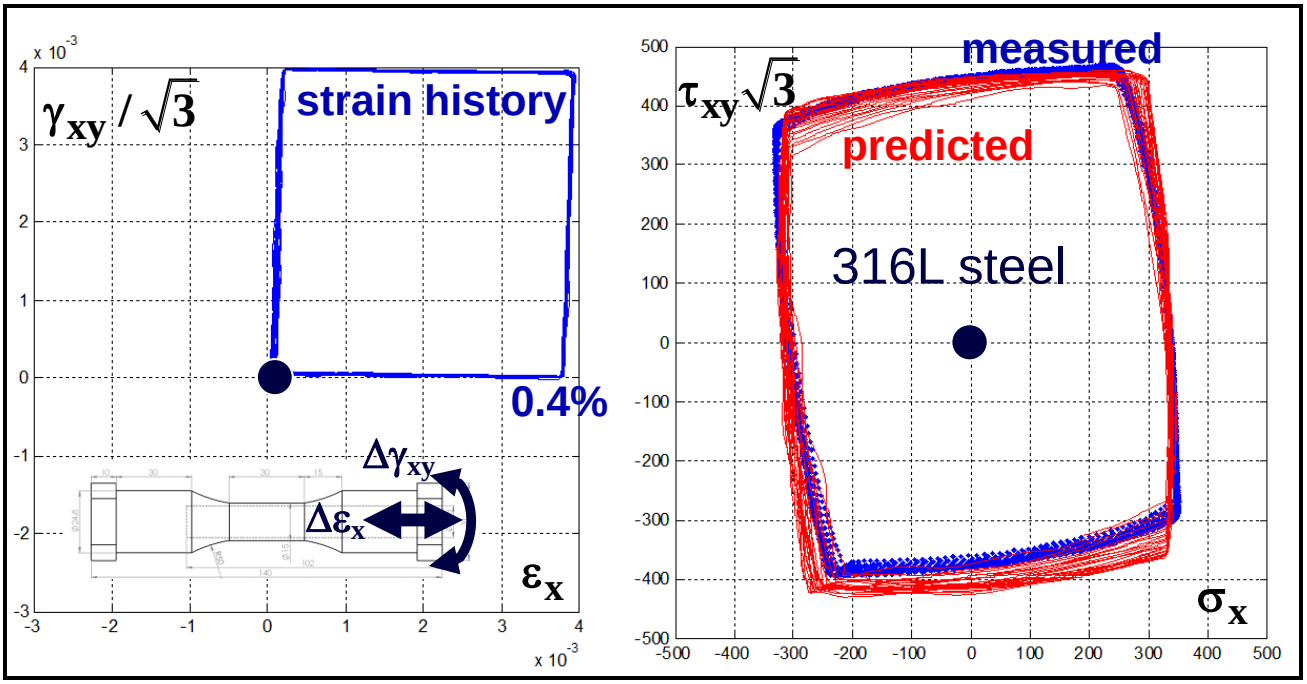

Fig. 6: Stress path predictions from the proposed formulation for a strain-controlled square pulse on a tension-torsion 316L steel tubular specimen, showing a good experimental agreement in the presence of significant mean stress relaxation.

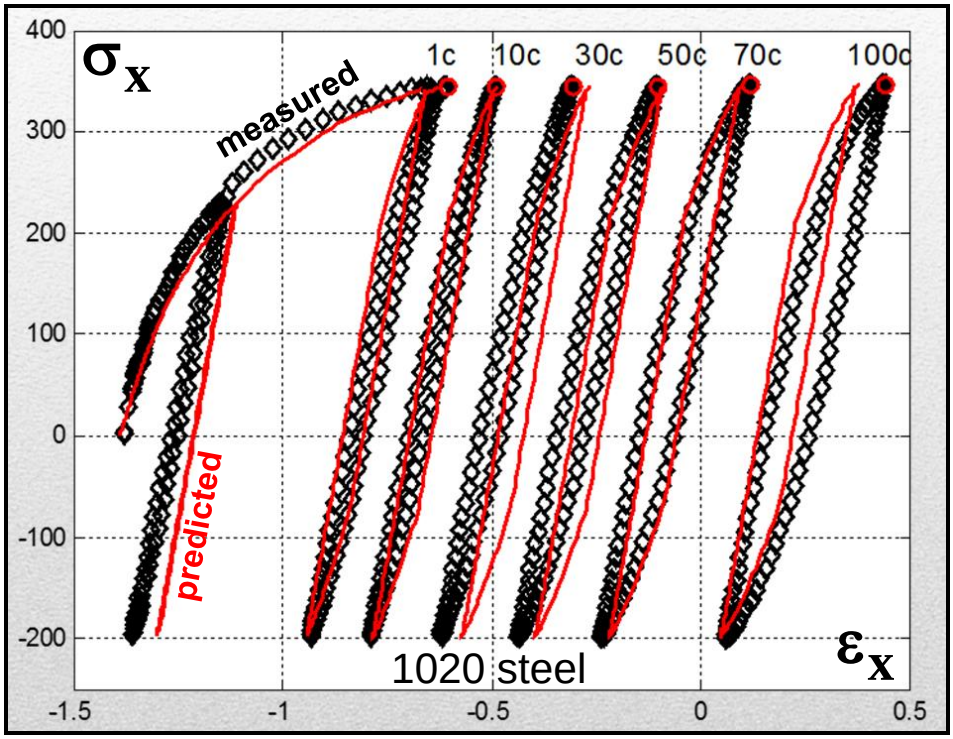

Fig. 7: Uniaxial ratcheting predictions from the proposed formulation for a 1020 steel cylindrical specimen, showing the predicted and measured uniaxial loops after 1, 10, 30, 50, 70, and 100 cycles.

Note that all tension-torsion simulations were performed in 2D sub-spaces of the proposed 5D stress and strain spaces, significantly decreasing computational cost, especially since both isotropic and NP hardening transients were considered. The simulations were repeated adopting a traditional 6D incremental plasticity formulation, resulting in the exact same path predictions but with a computational time about 100% higher than the one spent using the proposed formulation. Therefore, the proposed 5D framework is recommended due to its significantly lower computational cost, without any loss in calculation accuracy while considering isotropic and NP hardening transients, non-linear kinematic hardening, and notch effects.

8. Conclusions

In this work, an incremental plasticity formulation was proposed, entirely represented in efficient reduced-order five-dimensional (5D) stress and strain spaces. A generalized surface translation equation was proposed in 5D, from which all main non-linear kinematic (NLK) hardening models are a special case. The proposed 5D formulation can be easily transformed into 3D, 2D, or 1D representations of stresses and strains, to most efficiently calculate the stress-strain behavior under free-surface, tension-torsion, or uniaxial conditions, respectively. Such representations in lower dimensions can reduce in more than half the computational cost of incremental plasticity calculations, without altering the resulting predictions. Experiments with 316L and 1020 steel specimens confirmed the efficiency of the proposed framework to compute ratcheting and mean stress relaxation, which can have important effects on fatigue lives due to premature exhaustion of the material ductility and to changes in mean and maximum stresses.

Acknowledgments

This work was supported in part by the National Natural Science Foundation of P.R. China under Grant No. 11302150. CNPq-Brazil provided fellowships for Profs. Marco A. Meggiolaro and Jaime T.P. Castro, as well as a scholarship for Dr. Eleazar C.M. Sanchez.

References

[16] Ilyushin,AA, “On the foundations of the general mathematical theory of plasticity.” In: Voprosy Teorii Plastichnosti, Moskva: Izd. AN SSSR, p.3-29, 1961. (in Russian)

[17] Meggiolaro, M.A., Castro, J.T.P. An Improved Multiaxial Rainflow Algorithm for Non-Proportional Stress or Strain Histories - Part I: Enclosing Surface Methods. International Journal of Fatigue 2012;42:217-226.

[18] Meggiolaro, M.A., Castro, J.T.P. Prediction of non-proportionality factors of multiaxial histories using the Moment Of Inertia method. International Journal of Fatigue 2014;61:151-159.

[19] Meggiolaro, M.A., Castro, J.T.P. An Improved Multiaxial Rainflow Algorithm for Non-Proportional Stress or Strain Histories - Part II: The Modified Wang-Brown Method. International Journal of Fatigue 2012;42:194-206.

[20] Tanaka, E. A nonproportionality parameter and a cyclic viscoplastic constitutive model taking into account amplitude dependences and memory effects of isotropic hardening. European Journal of Mechanics - A/Solids 1994;13:155-173.

[21] Mróz, Z. On the description of anisotropic workhardening. Journal of the Mechanics and Physics of Solids 1967;15(3):163-175.

[22] Garud, Y.S. A new approach to the evaluation of fatigue under multiaxial loading. Transactions of the ASME Journal of Engineering Materials and Technology 1981;103:118-125.

[23] Krieg, R.D. A Practical Two-Surface Plasticity Theory. Journal of Applied Mechanics 1975;42(3):641-646.

[24] Dafalias, Y.F., Popov, E.P. Plastic internal variables formalism of cyclic plasticity. Journal of Applied Mechanics 1976;43(4):645-651.

[25] Chaboche, J.L. A review of some plasticity and viscoplasticity constitutive theories. International Journal of Plasticity 2008;24(10):1642-1693.

[26] Jiang, Y., Sehitoglu, H. Comments on the Mróz multiple surface type plasticity models. International Journal of Solids and Structures 1996;33(7):1053-1068.

[27] Armstrong, P.J., Frederick, C.O. A mathematical representation of the multiaxial Bauschinger effect. CEGB Report RD/B/N731, Berkeley Nuclear Laboratory, 1966.

[28] Chaboche, J.L., Dang Van, K., Cordier, G. Modelization of the Strain Memory Effect on the Cyclic Hardening of 316 Stainless Steel. Transactions of the Fifth International Conference on Structural Mechanics in Reactor Technology, Div. L, Berlin, 1979.

[29] Ohno, N., Wang, J.D. Transformation of a nonlinear kinematic hardening rule to a multisurface form under isothermal and nonisothermal conditions. International Journal of Plasticity 1991;7:879-891.

[30] Bari, S., Hassan, T. Kinematic hardening rules in uncoupled modeling for multiaxial ratcheting simulation. International Journal of Plasticity 2001;17(7):885-905.

[31] Jiang, Y., Kurath, P. Characteristics of the Armstrong-Frederick type plasticity models. International Journal of Plasticity 1996;12:387-415.

[32] Jiang, Y., Sehitoglu, H. Modeling of Cyclic Ratchetting Plasticity, Part I: Development of Constitutive Relations. ASME Journal of Applied Mechanics 1996;63(3):720-725.

[33] Prager, W. Recent developments in the mathematical theory of plasticity. Journal of Applied Physics 1949;20(3):235-241.

[34] Abdel Karim, M., Ohno, N. Kinematic Hardening Model Suitable for Ratcheting with Steady-State. International Journal of Plasticity 2000;16:225-240.

[35] Burlet, H., Cailletaud, G. Numerical techniques for cyclic plasticity at variable temperature. Engineering Computations 1986;3(2):143-153.

[36] Ohno, N., Wang, J.D. Kinematic hardening rules with critical state of dynamic recovery, Part I: formulations and basic features for ratchetting behavior. International Journal of Plasticity 1993;9:375-390.

[37] Ohno, N., Wang, J.D. Kinematic hardening rules with critical state of dynamic recovery, Part II: application to experiments of ratchetting behavior. International Journal of Plasticity 1993;9:391-403.

[38] Jiang, Y., Sehitoglu, H. Modeling of Cyclic Ratchetting Plasticity, Part II: Comparison of Model Simulations with Experiments. ASME Journal of Applied Mechanics 1996;63(3):726-733.

[39] Delobelle, P., Robinet, P., Bocher, L. Experimental Study and Phenomenological Modelization of Ratchet under Uniaxial and Biaxial Loading on an Austenitic Stainless Steel. International Journal of Plasticity 1995;11:295-330.

[40] Chen, X., Jiao, R., Kim, K.S. On the Ohno-Wang Kinematic Hardening Rules for Multiaxial Ratcheting Modeling of Medium Carbon Steel. International Journal of Plasticity 2005;21:161-184.

[41] Chen, X., Jiao, R. Modified kinematic hardening rule for multiaxial ratcheting prediction. International Journal of Plasticity 2004;20:871-898.

[42] Barkey, M.E., Socie, D.F., Hsia, K.J. A yield surface approach to the estimation of notch strain for proportional and nonproportional cyclic loading. Journal of Engineering Materials and Technology 1994;116:173-180.

[43] Molski, K., Glinka, G. A method of elastoplastic and strain calculation at a notch root. Materials Science and Engineering 1981;50:93-100.

[44] Kujawski, D. On energy interpretations of the Neuber's rule. Theoretical and Applied Fracture Mechanics 2014;73:91-96.

[45] Ince, A., Glinka, G. A Numerical Method for Elasto-Plastic Notch-Root Stress-Strain Analysis. Journal of Strain Analysis for Engineering Design 2013;48(4):229-224.

[46] McDonald, R.J., Socie, D.F. A technique to estimate the local multiaxial elastic-plastic behavior from a purely elastic solution. Engineering Fracture Mechanics 2011;78:1696-1704.

[47] Meggiolaro, M.A., Castro, J.T.P. Automation of the Fatigue Design under Variable Amplitude Loading Using the ViDa Software. International Journal of Structural Integrity 2010;1:1-6.

[48] Socie, D.F., Marquis, G.B. Multiaxial Fatigue, SAE 1999.